

The planetary theory of solar activity variability: a review

Nicola Scafetta¹ and Antonio Bianchini²

August 22, 2022

¹Department of Earth Sciences, Environment and Georesources, University of Naples Federico II, Complesso Universitario di Monte S. Angelo, via Cintia 21, 80126 Naples, Italy.

²INAF, Astronomical Observatory of Padua, Padua, Italy.

Email: nicola.scafetta@unina.it; antonio.bianchini@unipd.it

Abstract

Commenting the 11-year sunspot cycle, Wolf (1859, MNRAS 19, 85-86) conjectured that “*the variations of spot-frequency depend on the influences of Venus, Earth, Jupiter, and Saturn*”. The high synchronization of our planetary system is already nicely revealed by the fact that the ratios of the planetary orbital radii are closely related to each other through a scaling-mirror symmetry equation (Bank and Scafetta, Front. Astron. Space Sci. 8, 758184, 2022). Reviewing the many planetary harmonics and the orbital invariant inequalities that characterize the planetary motions of the solar system from the monthly to the millennial time scales, we show that they are not randomly distributed but clearly tend to cluster around some specific values that also match those of the main solar activity cycles. In some cases, planetary models have even been able to predict the time-phase of the solar oscillations including the Schwabe 11-year sunspot cycle. We also stress that solar models based on the hypothesis that solar activity is regulated by its internal dynamics alone have never been able to reproduce the variety of the observed cycles. Although planetary tidal forces are weak, we review a number of mechanisms that could explain how the solar structure and the solar dynamo could get tuned to the planetary motions. In particular, we discuss how the effects of the weak tidal forces could be significantly amplified in the solar core by an induced increase in the H-burning. Mechanisms modulating the electromagnetic and gravitational large-scale structure of the planetary system are also discussed.

Keywords: planetary systems, orbital synchronization, Solar cycles, Tidal forces, Mechanisms of solar variability

Cite as: Scafetta, N., Bianchini, A. (2022). The planetary theory of solar activity variability: a review. *Frontiers in Astronomy and Space Sciences*, Volume 9, Article 937930. <https://doi.org/10.3389/fspas.2022.937930>

1 Introduction

Since antiquity, the movements of the planets of the solar system have attracted the attention of astronomers and philosophers such as Pythagoras and Kepler because the orbital periods appeared to be related to each other by simple harmonic proportions, resonances, and/or commensurabilities (Haar, 1948; Stephenson, 1974). Such a philosophical concept is known as the “*Music of the Spheres*” or the “*Harmony of the Worlds*” (Godwin, 1992; Scafetta, 2014a). This property is rather common for many orbital systems (Agol et al., 2021; Aschwanden, 2018; Moons and Morbidelli, 1995; Scafetta, 2014a). Bank and Scafetta (2022) improved the Geddes and King-Hele equations describing the mirror symmetries among the orbital radii of the planets (Geddes and King-Hele, 1983) and discovered their ratios obey the following scaling-mirror symmetry relation

$$\begin{aligned} \frac{1}{64} \left(\frac{a_{Er}}{a_{Sz}} \right)^{\frac{2}{3}} &\approx \frac{1}{32} \left(\frac{a_{Pl}}{a_{Vu}} \right)^{\frac{2}{3}} \approx \frac{1}{16} \left(\frac{a_{Ne}}{a_{Me}} \right)^{\frac{2}{3}} \approx \frac{1}{8} \left(\frac{a_{Ur}}{a_{Ve}} \right)^{\frac{2}{3}} \\ &\approx \frac{1}{4} \left(\frac{a_{Sa}}{a_{Ea}} \right)^{\frac{2}{3}} \approx \frac{1}{2} \left(\frac{a_{Ju}}{a_{Ma}} \right)^{\frac{2}{3}} \approx 1 \left(\frac{a_{7:3}}{a_{3:1}} \right)^{\frac{2}{3}} \approx \frac{9}{8} \end{aligned} \quad (1)$$

where a_{planet} are the semi-major axes of the orbits of the relative planets: Eris (Er), Pluto (Pl), Neptune (Ne), Uranus (Ur), Saturn (Sa), Jupiter (Ju), Mars (Ma), Earth (Ea), Venus (Ve), Mercury (Me), Vulcanoid asteroid belt (Vu), and the scattered zone surrounding the Sun (Sz). See Figure 1. The ratio 9/8 is, musically speaking, a whole tone known as the Pythagorean *epogdoon*. The deviations of Eq. 1 from the actual orbital planetary ratios are within 1%.

Another intriguing aspect regarding the synchronization of the solar system is the fact that many planetary harmonics are found spectrally coherent with the solar activity cycles (e.g.: Scafetta, 2012a, 2020, and many others). The precise physical origin of solar cycles is still poorly known and dynamo models are debated, but recent literature has strengthened the hypothesis of a correlation with planetary harmonics. Actually, a few years after the discovery of the 11-year sunspot cycle, Wolf (1859) himself conjectured that “*the variations of spot-frequency depend on the influences of Venus, Earth, Jupiter, and Saturn*”. Dicke (1978) noted that the sunspot cycle shows no statistical indication of being randomly generated but rather of being synchronized by a chronometer hidden deep in the Sun. Solar activity is characterized by several cycles like the Schwabe 11-year sunspot cycle (Schwabe, 1843), the Hale solar magnetic 22-year cycle (Hale, 1908), the Gleissberg cycle (~85 years), the Jose cycle (~178 years), the Suess-de Vries cycle (~208 years), the Eddy cycle (~1000 years), and the Bray-Hallstatt cycle (~2300 years) (Abreu et al., 2012; McCracken et al., 2001, 2013; Scafetta, 2016). Shorter cycles are easily detected in total solar irradiance (TSI) and sunspot records, while the longer ones are detected in long-term geophysical records like the

cosmogenic radionuclide ones (^{14}C and ^{10}Be) and in climate records (Neff et al., 2001; Steinhilber et al., 2009). Planetary cycles have also been found in aurora records (Scafetta, 2012c; Scafetta and Willson, 2013a).

Due to the evident high synchronization of planetary motions, it is worthwhile investigating the possibility that orbital frequencies could tune solar variability as well. However, although Jupiter appears to play the main role in organizing the solar system (Bank and Scafetta, 2022), its orbital period (~11.86 years) is too long to fit the Schwabe 11-year solar cycle. Thus, any possible planetary mechanism able to create this solar modulation must involve a combination of more planets. We will see that the only frequencies that could be involved in the process are the orbital periods, the synodical periods, and their beats and harmonics.

In the following sections, we review the planetary theory of solar variability and show how it is today supported by many empirical and theoretical evidences at multiple timescales. We show that appropriate planetary harmonic models correlate with the 11-year solar cycle, the secular and millennial cycles, as well as with several other major oscillations observed in solar activity, and even with the occasional occurrences of solar flares. The physics behind these results is not yet fully understood, but a number of working hypotheses will be herein briefly discussed.

2 The solar dynamo and its open issues

The hypothesis we wish to investigate is whether the solar activity could be synchronized by harmonic planetary forcings. In principle, this could be possible because the solar structure itself is an oscillator. The solar cyclical magnetic activity can be explained as the result of a dynamo operating in the convective envelope or at the interface with the inner radiative region, where the rotational energy is converted into magnetic energy. Under certain conditions, in particular if the internal noise is sufficiently weak relative to the external forcing, an oscillating system could synchronize with a weak external periodic force, as first noted by Huygens in the 17th century (Pikovsky et al., 2001).

A comprehensive review of solar dynamo models is provided by Charbonneau (2020). In the most common α - Ω models, the magnetic field is generated by the combined effect of differential rotation and cyclonic convection. The mechanism starts with an initially poloidal magnetic field that is azimuthally stretched by the differential rotation of the convective envelope, especially at the bottom of the convective region (tachocline) where the angular velocity gradient is most steep. The continuous winding of the poloidal field lines (Ω mechanism) produces a magnetic toroidal field that accumulates in the boundary overshooting region. When the toroidal magnetic field and its magnetic pressure get

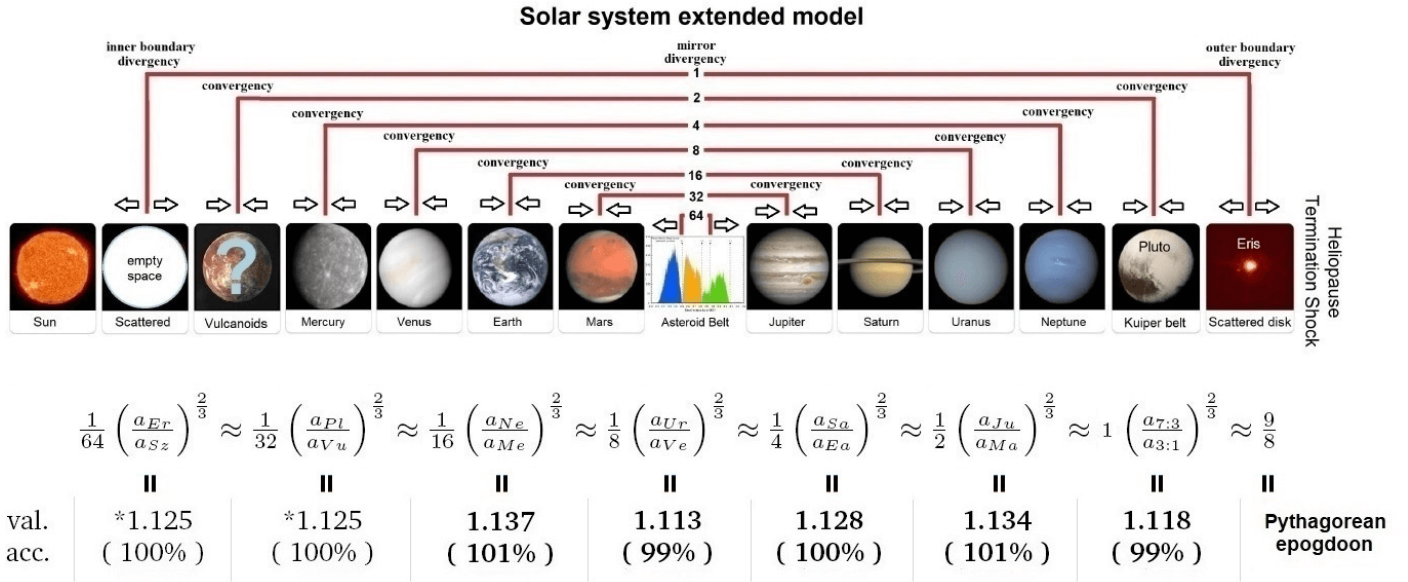


Figure 1: The following scaling-mirror symmetry relation among the semi-major axes of the orbits of the planets and asteroid belts of the solar system. (Bank and Scafetta, 2022).

strong enough, the toroidal flux ropes become buoyantly unstable and start rising through the convective envelope where they undergo helical twisting by the Coriolis forces (α mechanism) (Parker, 1955). When the twisted field lines emerge at the photosphere, they appear as bipolar magnetic regions (BMRs), that roughly coincide with the large sunspot pairs, also characterized by a dipole moment that is systematically tilted with respect to the E–W direction of the toroidal field. The turbulent decay of BMRs finally releases a N–S oriented fraction of the dipole moment that allows the formation of a global dipole field, characterized by a polarity reversal as required by the observations (Babcock–Leighton mechanism).

However, magneto-hydrodynamic simulations suggest that purely interface dynamos cannot be easily calibrated to solar observations, while flux-transport dynamos (based on the meridional circulation) are able to better simulate the 11-year solar cycle when the model parameters are calibrated to minimize the difference between observed and simulated time–latitude BMR patterns (Charbonneau, 2020; Dikpati and Gilman, 2007). Cole and Bushby (2014) showed that by changing the parameters of the MHD α - Ω dynamo models it is possible to obtain transitions from periodic to chaotic states via multiple periodic solutions. Macario-Rojas et al. (2018) obtained a reference Schwabe cycle of 10.87 years, which was also empirically found by Scafetta (2012a) by analyzing the sunspot record. This oscillation will be discussed later in the Jupiter-Saturn model of Sections 4.2 and 6.

Full MHD dynamo models are not yet available and several crucial questions are still open such as the stochastic and nonlinear nature of the dynamo, the formation of flux ropes and sunspots, the regeneration

of the poloidal field, the modulation of the amplitude and period of the solar cycles, how less massive fully convective stars with no tachocline may still show the same relationship between the rotation and magnetic activity, the role of meridional circulation, the origin of Maunder-type Grand Minima, the presence of very low-frequency Rieger-type periodicities probably connected with the presence of magneto-Rossby waves in the solar dynamo layer below the convection zone, and other issues (Zaqarashvili et al., 2010, 2021; Gurgenchvili et al., 2022).

3 The solar wobbling and its harmonic organization

The complex dynamics of the planetary system can be described by a general harmonic model. Any general function of the orbits of the planets – such as their barycentric distance, speed, angular momentum, etc. – must share a common set of frequencies with those of the solar motion (e.g.: Jose, 1965; Bucha et al., 1985; Cionco and Pavlov, 2018; Scafetta, 2010). Instead, the amplitudes and phases associated with each constituent harmonic depend on the specific chosen function.

Figure 2 (A and B) shows the positions and the velocities of the wobbling Sun with respect to the barycenter of the planetary system from BC 8002, to AD 9001 (100-day steps) calculated using the JPL’s HORIZONS Ephemeris system (Scafetta, 2010, 2014a).

We can analyze the main orbital frequencies of the planetary system by performing, for example, the harmonic analysis of the solar velocity alone. Its periodograms were obtained with the Fourier analysis (red)

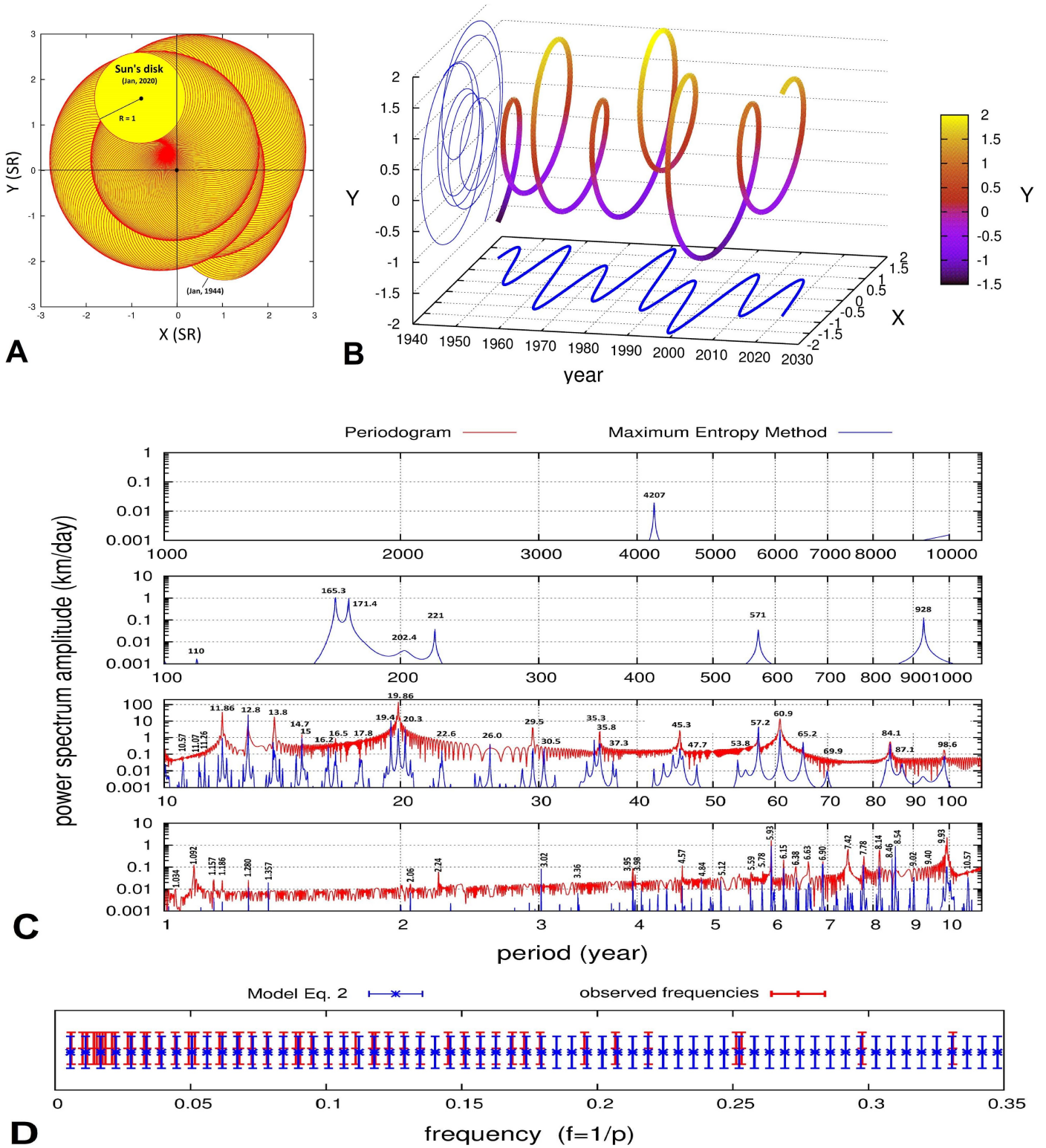


Figure 2: [A] The motion the wobbling Sun from 1944 to 2020 [B] The distance and the speed of the Sun relative to the barycenter of the solar system from 1800 to 2020. [C] Periodogram (red) and the maximum entropy method spectrum (blue) of the speed of the Sun from BC 8002-Dec-12, to AD 9001-Apr-24. [D] Comparison between the frequencies observed in [C] in the range 3 to 200 years (red) and the frequencies predicted by the harmonic model of Eq. 3 (blue). (cf. Scafetta, 2014a).

and the maximum entropy method (blue) (Press et al., 1997) and are shown in Figure 2C.

Several spectral peaks can be recognized: the ~ 1.092 year period of the Earth-Jupiter conjunctions; the

Planet	days	years
Mercury	87.969	0.241
Venus	224.701	0.615
Earth	365.256	1
Mars	686.980	1.881
Jupiter	4332.589	11.862
Saturn	10759.22	29.457
Uranus	30685.4	84.011
Neptune	60189.0	164.79

Table 1: Sidereal orbital periods of the planets of the solar system. From the Planetary Fact Sheet - Metric <https://nssdc.gsfc.nasa.gov/planetary/factsheet/>.

~ 9.93 and ~ 19.86 year periods of the Jupiter-Saturn spring (half synodic) and synodic cycles, respectively; the ~ 11.86 , ~ 29.5 , ~ 84 and ~ 165 years of the orbital periods of Jupiter, Saturn, Uranus and Neptune, respectively; the ~ 60 year cycle of the Trigon of Great Conjunctions between Jupiter and Saturn; the periods corresponding to the synodic cycles between Jupiter and Neptune (~ 12.8 year), Jupiter and Uranus (~ 13.8 year), Saturn and Neptune (~ 35.8 year), Saturn and Uranus (~ 45.3) and Uranus and Neptune (~ 171.4 year), as well as their spring periods.

The synodic period is defined as

$$P_{12} = \frac{1}{f_{12}} = \left| \frac{1}{P_1} - \frac{1}{P_2} \right|^{-1}, \quad (2)$$

where P_1 and P_2 are the orbital periods of two planets. Additional spectral peaks at ~ 200 - 220 , ~ 571 , ~ 928 and ~ 4200 years are also observed. The spring period is the half of P_{12} . The observed orbital periods are listed in Table 1.

Some of the prominent frequencies in the power spectra appear clustered around well-known solar cycles such as in the ranges 42-48 years, 54-70 years, 82-100 years (Gleissberg cycle), 155-185 (Jose cycle), and 190-240 years (Suess-de Vries cycle) (e.g.: Ogurtsov et al., 2002; Scafetta and Willson, 2013a). The sub-annual planetary harmonics and their spectral coherence with satellite total solar irradiance records will be discussed in Section 5.

The important result is that the several spectral peaks observed in the solar motion are not randomly distributed but are approximately reproduced using the following simple empirical harmonic formula

$$p_i = \frac{178.38}{i} \text{ yr}, \quad i = 1, 2, 3, \dots, \quad (3)$$

where 178 years corresponds to the period that Jose (1965) found both in the solar orbital motion and in the sunspot records (cf.: Jakubcová and Pick, 1986; Charvátová and Hejda, 2014). A comparison between the observed frequencies and those predicted by the harmonic model of Eq. 3 is shown in Figure 2D, where a strong coincidence is observed. Eq. 3 suggests that the solar

planetary system is highly self-organized and synchronized.

4 The Schwabe 11-year solar cycle

Wolf (1859) himself proposed that the ~ 11 -year sunspot cycle could be produced by the combined orbital motions of Venus, Earth, Jupiter and Saturn. In the following, we discuss two possible and complementary solar-planetary models made with the orbital periods of these four planets.

4.1 The Venus-Earth-Jupiter model

The first model relates the 11-year solar cycle with the relative orbital configurations of Venus, Earth and Jupiter, which was first proposed by Bendandi (1931) as recently reminded by Battistini (2011). Later, Bollinger (1952), Hung (2007) and others (e.g.: Scafetta, 2012c; Tattersall, 2013; Wilson, 2013; Stefani et al., 2016, 2019, 2021) developed more evolved models.

This model is justified by the consideration that Venus, Earth and Jupiter are the three major tidal planets (Scafetta, 2012b). Their alignments repeat every:

$$\frac{1}{f_{VEJ}} = P_{VEJ} = \left(\frac{3}{P_V} - \frac{5}{P_E} + \frac{2}{P_J} \right)^{-1} = 22.14 \text{ yr} \quad (4)$$

where $P_V = 224.701$ days, $P_E = 365.256$ days and $P_J = 4332.589$ days are the sidereal orbital periods of Venus, Earth and Jupiter, respectively.

The calculated 22.14-year period is very close to the ~ 22 -year Hale solar magnetic cycle. Since the Earth-Venus-Sun-Jupiter and Sun-Venus-Earth-Jupiter configurations present equivalent tidal potentials, the tidal cycle would have a recurrence of 11.07 years. This period is very close to the average solar cycle length observed since 1750 (Hung, 2007; Scafetta, 2012a; Stefani et al., 2016).

Vos et al. (2004) found evidence for a stable Schwabe cycle with a dominant 11.04-year period over a 1000-year interval which is very close to the above 11.07 periodicity, as suggested by Stefani et al. (2020a). However, the Jupiter-Saturn model also reproduces a similar Schwabe cycle (see Sections 4.2 and 6).

Eq. 4 is an example of “orbital invariant inequality” (Scafetta et al., 2016; Scafetta, 2020). Section 7 explains their mathematical property of being simultaneously and coherently seen by any region of a differentially rotating system like the Sun. This property should favor the synchronization of the internal solar dynamics with external forces varying with those specific frequencies.

Eq. 4 can be rewritten in a vectorial formalism as

$$(3, -5, 2) = 3(1, -1, 0) - 2(0, 1, -1). \quad (5)$$

Each vector can be interpreted a frequency where the order of its components correspond to the arbitrary assumed order of the planets, in this case: (Venus, Earth, Jupiter). Thus, $(3, -5, 2) \equiv 3/P_V - 5/P_E + 2/P_J$, $3(1, -1, 0) \equiv 3(1/P_V - 1/P_E)$ and $-2(0, 1, -1) \equiv -2(1/P_E - 1/P_J)$.

We observe that $(1, -1, 0)$ indicates the frequency of the synodic cycle between Venus and Earth and $(0, 1, -1)$ indicates the frequency of the synodic cycle between Earth and Jupiter (Eq. 2). Thus, the vector $(3, -5, 2)$ indicates the frequency of the beat created by the third harmonic of the synodic cycle between Venus and Earth and the second harmonic of the synodic cycle between Earth and Jupiter.

Eq. 5 also means that the Schwabe sunspot cycle can be simulated by the function:

$$f(t) = \cos\left(2\pi \cdot 2 \cdot 3 \frac{t - t_{VE}}{P_{VE}}\right) + \cos\left(2\pi \cdot 2 \cdot 2 \frac{t - t_{EJ}}{P_{EJ}}\right), \quad (6)$$

where $t_{VE} = 2002.8327$ is the epoch of a Venus-Earth conjunction whose period is $P_{VE} = 1.59867$ years; and $t_{EJ} = 2003.0887$ is the epoch of an Earth-Jupiter conjunction whose period is $P_{EJ} = 1.09207$ years. The 11.07-year beat is obtained by doubling the synodic frequencies given in Eq. 5.

Figure 3A shows that the three-planet model of Eq. 6 (red) generates a beat pattern of 11.07 years reasonably in phase with the sunspot cycle (blue). More precisely, the maxima of the solar cycles tend to occur when the perturbing forcing produced by the beat is stronger, that is when the spring tides of the planets can interfere constructively somewhere in the solar structure.

Hung (2007) and Scafetta (2012a) developed the three-planet model by introducing a three-planetary alignment index. In the case of two planets, the alignment index I_{ij} between planet i and planet j is defined as:

$$I_{ij} = |\cos(\Theta_{ij})|, \quad (7)$$

where Θ_{ij} is the angle between the positions of the two planets relative to the solar center.

Eq. 7 indicates that when the two planets are aligned ($\Theta_{ij} = 0$ or $\Theta_{ij} = \pi$), the alignment index has the largest value because these two positions imply a spring-tide configuration. Instead, when $\Theta_{ij} = \pi/2$, the index has the lowest value because at right angles – corresponding to a neap-tide configuration – the tides of the two planets tend to cancel each other.

In the case of the Venus-Earth-Jupiter system, there are three correspondent alignment indexes:

$$I_V = |\cos(\Theta_{VE})| + |\cos(\Theta_{VJ})| \quad (8)$$

$$I_E = |\cos(\Theta_{EV})| + |\cos(\Theta_{EJ})| \quad (9)$$

$$I_J = |\cos(\Theta_{JV})| + |\cos(\Theta_{JE})|. \quad (10)$$

Then, the combined alignment index I_{VEJ} for the three planets could be defined as:

$$I_{VEJ} = \text{smallest among } (I_V, I_E, I_J), \quad (11)$$

which ranges between 0 and 2.

Figure 3B shows (in red) that the number of the most aligned days of Venus, Earth and Jupiter – estimated by Eq. 11 – presents an 11.07-year cycle. These cycles are well correlated, both in phase and frequency, with the ~ 11 -year sunspot cycle. Scafetta (2012a) also showed that an 11.08-year recurrence exists also in the amplitude and direction (latitude and longitude components) of the solar jerk-shock vector, which is the time-derivative of the acceleration vector. For additional details see Hung (2007), Scafetta (2012a), Salvador (2013), Wilson (2013) and Tattersall (2013).

A limitation of the Venus-Earth-Jupiter model is that it cannot explain the secular variability of the sunspot cycle which alternates prolonged low and high activity periods such as, for example, the Maunder grand solar minimum between 1645 and 1715, when very few sunspots were observed (cf. Smythe and Eddy, 1977). However, this problem could be solved by the Jupiter-Saturn model (Scafetta, 2012a) discussed below and, in general, by taking into account also the other planets (Scafetta, 2020; Stefani et al., 2021), as discussed in Sections 6 and 7.

The 11.07-year cycle has also been extensively studied by Stefani et al. (2016); Stefani (2018); Stefani et al. (2019, 2020b, 2021) where it is claimed to be the fundamental periodicity synchronizing the solar dynamo.

4.2 The Jupiter-Saturn model

The second model assumes that the Schwabe sunspot cycle is generated by the combined effects of the planetary motions of Jupiter and Saturn. The two planets generate two main tidal oscillations associated with the orbit of Jupiter (11.86-year period) – which is characterized by a relatively large eccentricity ($e = 0.049$) – and the spring tidal oscillation generated by Jupiter and Saturn (9.93-year period) (Brown, 1900; Scafetta, 2012c). In this case, the Schwabe sunspot cycle could emerge from the synchronization of the two tides with periods of 9.93 and 11.86 years, whose average is about 11 years.

The Jupiter-Saturn model is supported by a large number of evidences. For example, Scafetta (2012a,b) showed that the sunspot cycle length – i.e. the time between two consecutive sunspot minima – is bi-modally distributed, being always characterized by two peaks at periods smaller and larger than 11 years. This suggests that there are two dynamical attractors at the periods of about 10 and 12 years forcing the sunspot cycle length to fall either between 10 and 11 years or between 11 and 12 years. Sunspot cycles with a length very close to 11 years are actually absent. In addition, Figures 3C and D show the periodograms of the monthly sunspot record

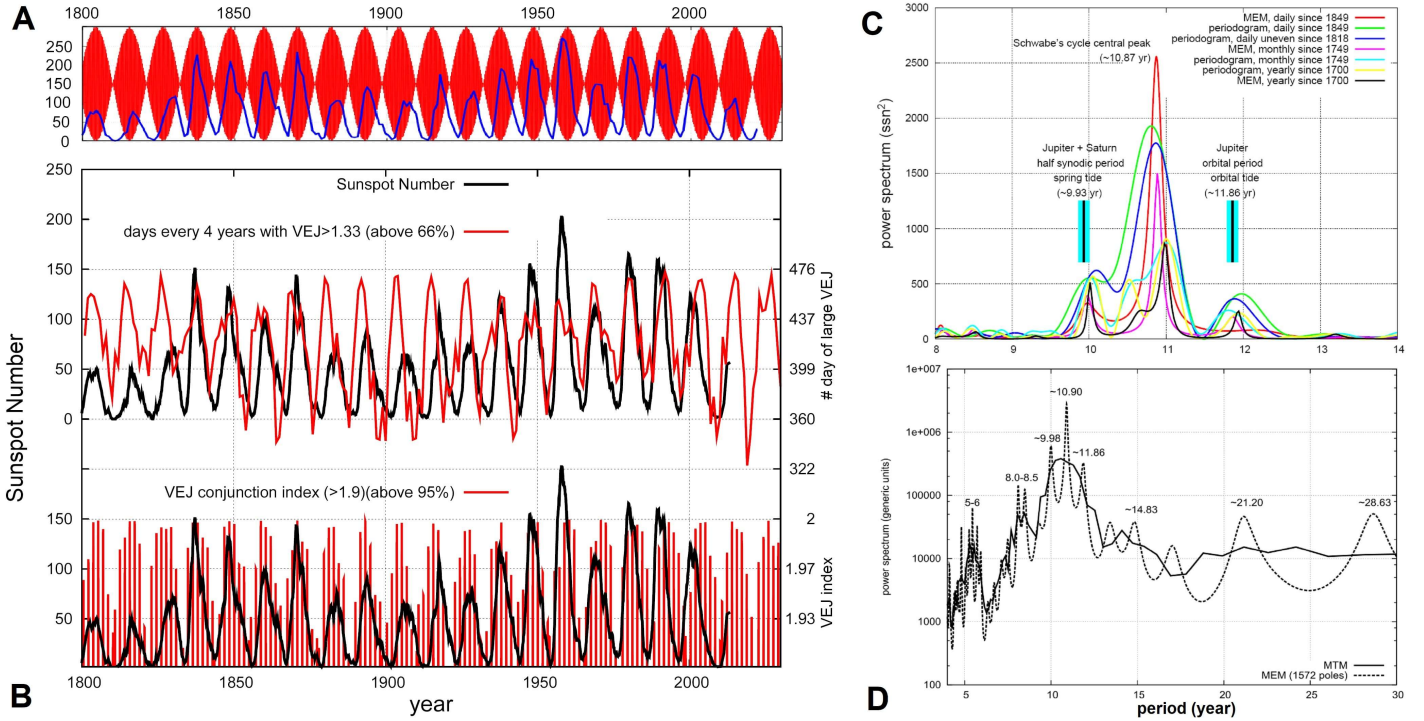


Figure 3: [A] The plot of Eq. 6 (red) versus the sunspot number record (blue). [B, Top] The sunspot number record (black) versus the alignment index $I_{VEJ} > 66\%$. [B, Bottom] The sunspot number record (black) against the number of days of most alignment ($I_{VEJ} > 95\%$) (red). [C and D] Power spectra of the Schwabe sunspot cycle using the Maximum Entropy Method (MEM) and the periodogram (MTM) (Press et al., 1997). (Data from: <https://www.sidc.be/silso/datafiles>).

since 1749. The spectral analysis of this long record reveals the presence of a broad major peak at about 10.87 years obtained by some solar dynamo models (Macario-Rojas et al., 2018) which is surrounded by two minor peaks at 9.93 and 11.86 years that exactly correspond with the two main tides of the Jupiter-Saturn system.

In Section 6 we will show that the combination of these three harmonics produces a multidecadal, secular and millennial variability that is rather well correlated with the long time-scale solar variability.

5 Solar cycles shorter than the Schwabe 11-year solar cycle

On small time scales, Bigg (1967) found an influence of Mercury on sunspots. Indeed, in addition to Jupiter, Mercury can also induce relatively large tidal cycles on the Sun because its orbit has a large eccentricity ($e = 0.206$) (Scafetta, 2012a).

Rapid oscillations in the solar activity can be optimally studied using the satellite total solar irradiance (TSI) records. Since 1978, TSI data and their composites have been obtained by three main independent science teams: ACRIMSAT/ACRIM3 (Willson and Mordvinov, 2003), SOHO/VIRGO (Fröhlich, 2006) and SORCE/TIM (Kopp and Lawrence, 2005a; Kopp et al., 2005b). Figure 4 compares the ACRIM3, VIRGO and

TIM TSI from 2000 to 2014; the average irradiance is about 1361 W/m^2 .

5.1 The 22-40 days time-scale

Figure 4B shows the power spectra in the 22-40 days range of the three TSI records (Figure 4A) from 2003.15 to 2011.00 (Scafetta and Willson, 2013c). A strong spectral peak is observed at ~ 27.3 days (0.075 years) (Willson and Mordvinov, 1999), which corresponds to the synodic period between the Carrington solar rotation period of ~ 25.38 days and the Earth's orbital period of ~ 365.25 days. The Carrington period refers to the rotation of the Sun at 26° of latitude, where most sunspots form and the solar magnetic activity emerges (Bartels, 1934). The observed 27.3-day period differs from the Carrington 25.38-day period because the Sun is seen from the orbiting Earth. Thus, the 27.3-day period derives from Eq. 2 using $T_1 = 25.38$ days and $T_2 = 365.25$ days.

Figure 4B reveals additional spectral peaks at ~ 24.8 days (~ 0.068 years), ~ 34 -35 days (~ 0.093 -0.096 years), and ~ 36 -38 days (~ 0.099 -0.104 years). They fall within the range of the solar differential rotation that varies from 24.7-25.4 days near the equator (Kotov, 2020) to about 38 days near the poles (Beck, 2000).

However, the same periods appear to be also associated with the motion of the planets. In fact, the ~ 24.8 -

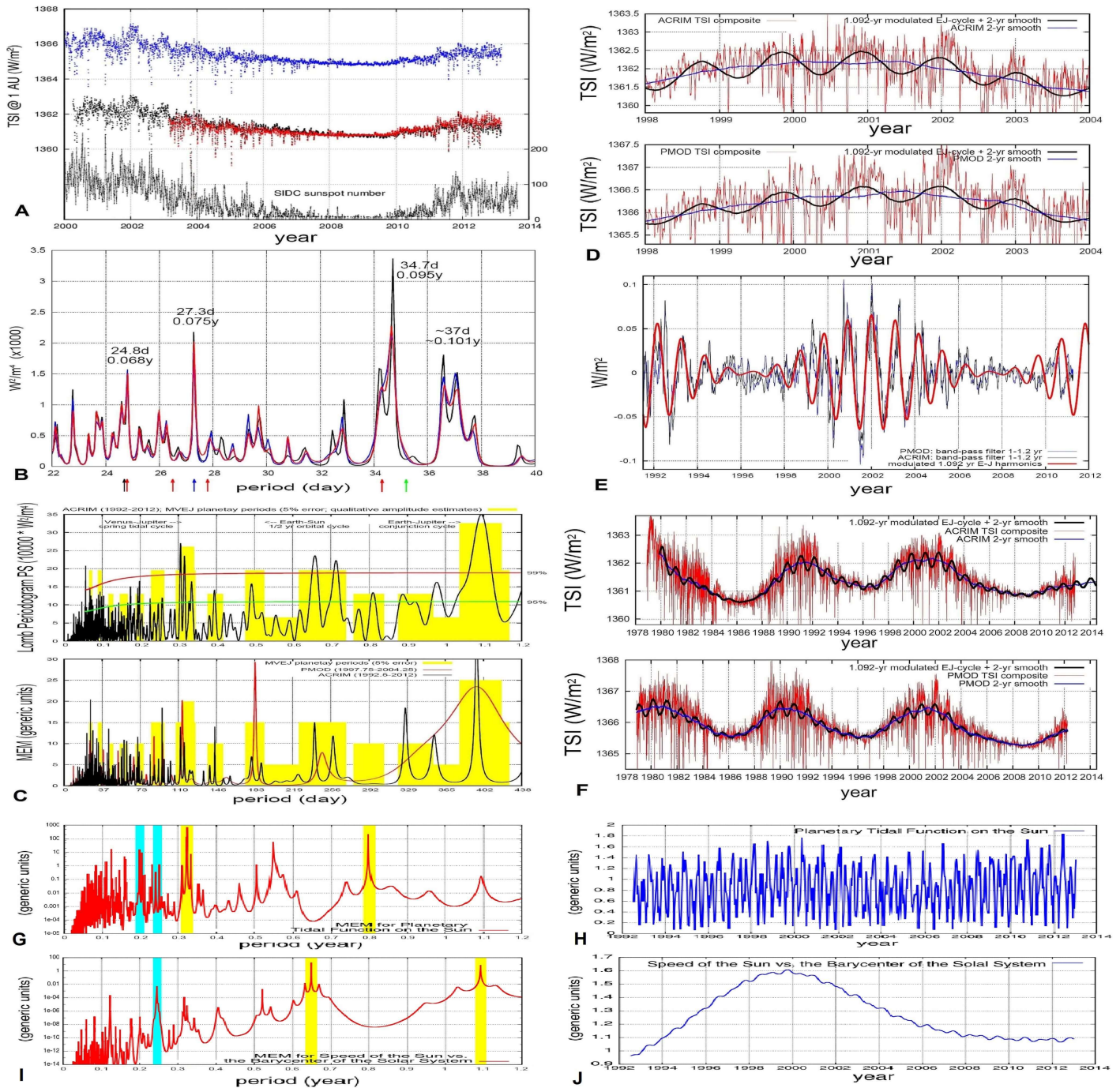


Figure 4: [A] Comparison of ACRIMSAT/ACRIM3 (black), SOHO/VIRGO (blue) and SORCE/TIM (red) TSI records versus daily sunspot number (gray). [B] Power spectrum comparison of ACRIMSAT/ACRIM3 (black), SOHO/VIRGO (blue) and SORCE/TIM (red) TSI from 2003.15 to 2011.00. The arrows at the bottom depicts the periods reported in Table 2. [C, Top] Periodogram of ACRIM results in W^2/m^4 from 1992.5-2012. [C, Bottom] Power spectra of ACRIM from 1992.5 to 2012.9) and of PMOD from 1997.75 to 2004.25. The yellow bars schematically indicate the harmonics generated by the planets as reported in Tables 2, 3 and 4. [D] ACRIM and PMOD TSI composites during solar maximum 23 (1998-2004). The black curve is from Eqs. 7 and 8. [E] High-pass filter of the PMOD (blue) and ACRIM (black) TSI compared against a 1.092-year harmonic Jupiter function (red).. [F] ACRIM and PMOD TSI since 1978 (red) against the models of Eqs. 13 and 14. [G, H] Planetary tidal function on the Sun (blue) (see Figure 9C) and its power spectrum (red). [I, J] Speed of the Sun relative to the solar system barycenter (blue) and its power spectrum (red). (cf. Scafetta and Willson, 2013b,c).

day cycle corresponds to the synodic period between the

sidereal orbital period of Jupiter (~ 4332.6 days) and the

Cycle	Type	P (day)	P (year)	color
Sun	equ-rot	24.7	0.0676	black
Sun – Ju	equ-rot	24.8	0.0679	red
Sun – Ea	equ-rot	26.5	0.0726	red
Sun – Ea	Car-rot	27.3	0.0747	blue
Sun – Ve	equ-rot	27.8	0.0761	red
Sun – Me	equ-rot	34.3	0.0940	red
2/5 Me	resonance	35.2	0.0964	green

Table 2: Solar equatorial (equ-) and Carrington (Car-) rotation cycles relative to the fixed stars and to the four major tidally active planets calculated using Eq. 2 where $P_1 = 24.7$ days is the sidereal equatorial solar rotation and P_2 the orbital period of a planet. Last column: color of the arrows in Figure 4B. (cf. Scafetta and Willson, 2013c).

sidereal equatorial rotation period of the Sun (~ 24.7 days) calculated using Eq. 2. Additional synodic cycles between the rotating solar equator and the orbital motion of the terrestrial planets are calculated at ~ 26.5 days, relative to the Earth, ~ 27.75 days, relative to Venus, and ~ 34.3 days, relative to Mercury (see Table 2). We also notice that the major TSI spectral peak at 34.7 days is very close to the ~ 34.3 -day Mercury-Sun synodic period, although it would require the slightly different solar rotation period of 24.89 days.

5.2 The 0.1-1.1 year time-scale

Tables 3 and 4 collect the orbital periods, the synodic cycles and their harmonics among the terrestrial planets (Mercury, Venus, Earth and Mars). The tables also show the synodic cycles between the terrestrial and the Jovian planets (Jupiter, Saturn, Uranus, and Neptune). The calculated periods are numerous and clustered. If solar activity is modulated by planetary motions, these frequency clusters should be observed also in the TSI records.

Figure 4C shows two alternative power spectra of the ACRIM and PMOD TSI records superposed to the distribution (yellow) of the planetary frequencies reported in Tables 2, 3 and 4. The main power spectral peaks are observed at: ~ 0.070 , ~ 0.097 , ~ 0.20 , ~ 0.25 , 0.30 - 0.34 , ~ 0.39 , ~ 0.55 , 0.60 - 0.65 , 0.7 - 0.9 , and 1.0 - 1.2 years.

Figure 4C shows that all the main spectral peaks observed in the TSI records appear compatible with the clusters of the calculated orbital harmonics. For example: the Mercury-Venus spring-tidal cycle (0.20 years); the Mercury orbital cycle (0.24 years); the Venus-Jupiter spring-tidal cycle (0.32 years); the Venus-Mercury synodic cycle (0.40 years); the Venus-Jupiter synodic cycle (0.65 years); and the Venus-Earth spring tidal cycle (0.80 years). A 0.5-year cycle is also observed, which could be due to the Earth crossing the solar equatorial plane twice a year and to a latitudinal dependency of the solar luminosity. These results are also confirmed by the power spectra of the planetary tidal function on

the Sun (see Figure 9C) and of the speed of the Sun relative to the solar system barycenter (Figures 4G-J).

The 1.0-1.2 year band observed in the TSI records correlates well with the 1.092-year Earth-Jupiter synodic cycle. Actually, the TSI records present maxima in the proximity of the Earth-Jupiter conjunction epochs (Scafetta and Willson, 2013b).

Figure 4D shows the ACRIM and PMOD TSI records (red curves) plotted against the Earth-Jupiter conjunction cycles with the period of 1.092 years (black curve) from 1998 to 2004. TSI peaks are observed around the times of the conjunctions. The largest peak occurs at the beginning of 2002 when the conjunction occurred at a minimum of the angular separation between Earth and Jupiter ($0^\circ 13' 19''$).

Figure 4E shows the PMOD (blue) and ACRIM (black) records band-pass filtered to highlight the 1.0-1.2 year modulation. The two curves (blue and black) are compared to the 1.092-year harmonic function (red):

$$f(t) = g(t) \cos \left[2\pi \frac{(t - 2002)}{1.09208} \right], \quad (12)$$

where the amplitude $g(t)$ was modulated according to the observed Schwabe solar cycle. The time-phase of the oscillation is chosen at $t_{EJ} = 2002$ because one of the Earth-Jupiter conjunctions occurred on the 1st of January, 2002. The average Earth-Jupiter synodic period is 1.09208 years. The TSI 1.0-1.2 year oscillation is significantly attenuated during solar minima (1995-1997 and 2007-2009) and increases during solar maxima. In particular, the figure shows the maximum of solar cycle 23 and part of the maxima of cycles 22 and 24 and confirms that the TSI modulation is well correlated with the 1.092-year Earth-Jupiter conjunction cycle.

Figure 4F extends the model prediction back to 1978. Here the TSI records are empirically compared against the following equations:

for ACRIM,

$$f(t) = S_A(t) + 0.2(S_A(t) - 1360.58) \cos \left[2\pi \frac{(t - 2002)}{1.09208} \right]; \quad (13)$$

for PMOD,

$$f(t) = S_P(t) + 0.2(S_P(t) - 1365.3) \cos \left[2\pi \frac{(t - 2002)}{1.09208} \right]. \quad (14)$$

The blue curves are the 2-year moving averages, $S_A(t)$ and $S_P(t)$, of the ACRIM and PMOD TSI composite records, respectively. The data-model comparison confirms that the 1.092-year Earth-Jupiter conjunction cycle is present since 1978. In fact, TSI peaks are also found in coincidences with a number of Earth-Jupiter conjunction epochs like those of 1979, 1981, 1984, 1990, 1991, 1992, 1993, 1994, 1995, 1998, 2011 and 2012. The 1979 and 1990 peaks are less evident in the PMOD TSI record, likely because of the significant modifications

Cycle	Type	P (day)	P (year)	min (year)	max (year)
Me	$1/2$ orbital	44 ± 0	0.1205 ± 0.000	0.1205	0.1205
Me – Ju	spring	45 ± 9	0.123 ± 0.024	0.090	0.156
Me – Ea	spring	58 ± 10	0.159 ± 0.027	0.117	0.189
Me – Ve	spring	72 ± 8	0.198 ± 0.021	0.156	0.219
Me	orbital	88 ± 0	0.241 ± 0.000	0.241	0.241
Me – Ju	synodic	90 ± 1	0.246 ± 0.002	0.243	0.250
Ea	$1/4$ orbital	91 ± 3	0.25 ± 0.000	0.250	0.250
Ve	$1/2$ orbital	112.5 ± 0	0.3075 ± 0.000	0.3075	0.3075
Me – Ea	synodic	116 ± 9	0.317 ± 0.024	0.290	0.354
Ve – Ju	spring	118 ± 1	0.324 ± 0.003	0.319	0.328
Ea	$1/3$ orbital	121 ± 7	0.333 ± 0.000	0.333	0.333
Me – Ve	synodic	145 ± 12	0.396 ± 0.033	0.342	0.433
Ea	$1/2$ orbital	182 ± 0	0.500 ± 0.000	0.5	0.5
Ea – Ju	spring	199 ± 3	0.546 ± 0.010	0.531	0.562
Ve	orbital	225 ± 0	0.615 ± 0.000	0.241	0.241
Ve – Ju	synodic	237 ± 1	0.649 ± 0.004	0.642	0.654
Ve – Ea	spring	292 ± 3	0.799 ± 0.008	0.786	0.810
Ea	orbital	365.25 ± 0	1.000 ± 0.000	1.000	1.000
Ea – Ju	synodic	399 ± 3	1.092 ± 0.009	1.082	1.104
Ea – Ve	synodic	584 ± 6	1.599 ± 0.016	1.572	1.620

Table 3: Major theoretical planetary harmonics with period $P < 1.6$ years. The synodic period is given by Eq. 2; the spring period is half of it. (cf. Scafetta and Willson, 2013c).

of the published Nimbus7/ERB TSI record in 1979 and 1989-1990 proposed by the PMOD science team (Fröhlich, 2006; Scafetta, 2009; Scafetta et al., 2011).

The result suggests that the side of the Sun facing Jupiter could be slightly brighter, in particular during solar maxima. Thus, when the Earth crosses the Sun-Jupiter line, it could receive an enhanced amount of radiation. This coalesces with strong hotspots observed on other stars with orbiting close giant planets (Shkolnik et al., 2003, 2005). Moreover, Kotov and Haneychuk (2020) analyzed 45 years of observations and showed that the solar photosphere, as seen from the Earth, is pulsating with two fast and relatively stable periods $P_0 = 9,600.606(12)$ s and $P_1 = 9,597.924(13)$ s. Their beatings occur with a period of 397.7(2.6) days, which coincides well with the synodic period between Earth and Jupiter (398.9 days). A hypothesis was advanced that the gravity field of Jupiter could be involved in the process.

5.3 The solar cycles in the 2-9 year range

The power spectrum in Figure 3D shows peaks at 5-6 and 8.0-8.5 years. The former ones appear to be harmonics of the Schwabe 11-year solar cycle discussed in Section 3. The latter peaks are more difficult to be identified. In any case, some planetary harmonics involving Mercury, Venus, Earth, Jupiter and Saturn could explain them.

For example, the Mercury-Venus orbital combination repeats almost every 11.08 years, which is similar to the 11.07-year invariant inequality between Venus, Earth and Jupiter discussed in Section 3. In fact, $P_M = 0.241$

years and $P_V = 0.615$ years, therefore their closest geometrical recurrences occur after 23 orbits of Mercury ($23P_M = 5.542$ years) and 9 orbits of Venus ($9P_V = 5.535$ year). Moreover, we have $46P_M = 11.086$ years and $18P_V = 11.07$ years. Thus, the orbital configuration of Mercury and Venus repeats every 5.54 years as well as every 11.08 years and might contribute to explain the 5-6 years spectral peak observed in Figure 3D. Moreover, 8 orbits of the Earth ($8P_E = 8$ years) and 13 orbits of Venus ($13P_V = 7.995$ years) nearly coincide and this combination might have contributed to produce the spectral peak at about 8 years.

There is also the possibility that the harmonics at about 5.5 and 8-9 years could emerge from the orbital combinations of Venus, Earth, Jupiter and Saturn. In fact, we have the following orbital invariant inequalities

$$\left(\frac{2}{P_V} - \frac{3}{P_E} - \frac{2}{P_J} + \frac{3}{P_S} \right)^{-1} = 5.43 \text{ yr} \quad (15)$$

and

$$2 \left(-\frac{1}{P_V} + \frac{2}{P_E} - \frac{2}{P_J} + \frac{1}{P_S} \right)^{-1} = 8.34 \text{ yr}, \quad (16)$$

where the orbital periods of the four planets are given in Table 1. Eq. 15 combines the spring cycle between Venus and Jupiter with the third harmonic of the synodic cycle between Earth and Saturn. Eq. 16 is the first inferior harmonic (because of the factor 2) of a combination of the synodic cycle between Venus and Saturn and the spring cycle between Earth and Jupiter. Eqs. 15 and 16 express orbital invariant inequalities, whose general physical properties are discussed in Section 7.

Cycle	Type	P (year)	Type	P (year)
Me – Ne	spring	0.1206	synodic	0.2413
Me – Ur	spring	0.1208	synodic	0.2416
Me – Sa	spring	0.1215	synodic	0.2429
Me – Ma	spring	0.1382	synodic	0.2763
Ve – Ne	spring	0.3088	synodic	0.6175
Ve – Ur	spring	0.3099	synodic	0.6197
Ve – Sa	spring	0.3142	synodic	0.6283
Ve – Ma	spring	0.4571	synodic	0.9142
Ea – Ne	spring	0.5031	synodic	1.006
Ea – Ur	spring	0.5060	synodic	1.0121
Ea – Sa	spring	0.5176	synodic	1.0352
Ea – Ma	spring	1.0676	synodic	2.1352
Ma	1/2 orbital	0.9405	orbital	1.8809
Ma – Ne	spring	0.9514	synodic	1.9028
Ma – Ur	spring	0.9621	synodic	1.9241
Ma – Sa	spring	1.0047	synodic	2.0094
Ma – Ju	spring	1.1178	synodic	2.2355
Ju	1/2 orbital	5.9289	orbital	11.858
Ju – Ne	spring	6.3917	synodic	12.783
Ju – Ur	spring	6.9067	synodic	13.813
Ju – Sa	spring	9.9310	synodic	19.862
Sa	1/2 orbital	14.712	orbital	29.424
Sa – Ne	spring	17.935	synodic	35.870
Sa – Ur	spring	22.680	synodic	45.360
Ur	1/2 orbital	41.874	orbital	83.748
Ur – Ne	spring	85.723	synodic	171.45
Ne	1/2 orbital	81.862	orbital	163.72
Me – (Ju – Sa)	spring	0.122	synodic	0.244
Me – (Ea – Ju)	spring	0.155	synodic	0.309
Ve – (Ju – Sa)	spring	0.317	synodic	0.635
Ea – (Ju – Sa)	spring	0.527	synodic	1.053
Ve – (Ea – Ju)	spring	0.704	synodic	1.408

Table 4: Additional expected harmonics associated with planetary orbits. The last five rows report the synodic and spring periods of Mercury, Venus and Earth relative to the Jupiter-Saturn and Earth-Jupiter synodic periods calculated as $P_{1(23)} = 1/|1/P_1 - |1/P_2 - 1/P_3||$. (cf. Scafetta and Willson, 2013b,c).

The above results, together with those discussed in Section 4, once again suggest that the major features of solar variability at the decadal scale from 2 to 22 years could have been mostly determined by the combined effect of Venus, Earth, Jupiter and Saturn, as it was first speculated by Wolf (1859).

6 The multi-decadal and millennial solar cycles predicted by the Jupiter-Saturn model

As discussed in Section 4.1, the Jupiter-Saturn model interprets quite well two of the three main periods that characterize the sunspot number record since 1749: $P_{S1} = 9.93$, $P_{S2} = 10.87$ and $P_{S3} = 11.86$ years (Figure 3C) (Scafetta, 2012a). The two side frequencies match the spring tidal period of Jupiter and Saturn (9.93 years), and the tidal sidereal period of Jupiter

(11.86 years). The central peak at $P_{S2} = 10.87$ years can be associated with a possible natural dynamo frequency that is also predicted by a flux-transport dynamo model (Macario-Rojas et al., 2018). However, the same periodicity could be also interpreted as twice the invariant inequality period of Eq. 15, which gives 10.86 years. According to the latter interpretation, the central frequency sunspot peak might derive from a dynamo synchronized by a combination of the orbital motions of Venus, Earth, Jupiter and Saturn.

The three harmonics of the Schwabe frequency band beat at $P_{S13} = 60.95$ years, $P_{S12} = 114.78$ years and $P_{S23} = 129.95$ years. Using the same vectorial formalism introduced in Section 3.1 to indicate combinations of synodical cycles, a millennial cycle, P_{S123} , is generated by the beat between $P_{S12} \equiv (1, -1, 0)$ and $P_{S23} \equiv (0, 1, -1)$ according to the equation $(1, -1, 0) - (0, 1, -1) = (1, -2, 1)$ that corresponds to the period

$$P_{S123} = \left(\frac{1}{P_{S1}} - \frac{2}{P_{S2}} + \frac{1}{P_{S3}} \right)^{-1} \approx 983 \text{ yr}, \quad (17)$$

where we adopted the multi-digits accurate values $P_{S1} = 9.929656$ years, $P_{S2} = 10.87$ years and $P_{S3} = 11.862242$ years (Table 1). However, the millennial beat is very sensitive to the choice of P_{S2} .

To test whether this three-frequency model actually fits solar data, Scafetta (2012a) constructed its constituent harmonic functions by setting their relative amplitudes proportional to the power of the spectral peaks of the sunspot periodogram. The three amplitudes, normalized with respect to A_{S2} , are: $A_{S1} = 0.83$, $A_{S2} = 1$, $A_{S3} = 0.55$.

The time-phases of the two side harmonics are referred to: $t_{S1} = 2000.475$, which is the synodic conjunction epoch of Jupiter and Saturn (23/June/2000) relative to the Sun, when the spring tide must be stronger; and $t_{S3} = 1999.381$, which is the perihelion date of Jupiter (20/May/1999) when its tide is stronger. The time-phase of the central harmonic was set to $t_{S2} = 2002.364$ and was estimated by fitting the sunspot number record with the three-harmonic model keeping the other parameters fixed.

The time-phases of the beat functions are calculated using the equation

$$t_{12} = \frac{P_2 t_1 - P_1 t_2}{P_2 - P_1}. \quad (18)$$

It was found $t_{S12} = 2095.311$, $t_{S13} = 2067.044$ and $t_{S23} = 2035.043$. The time-phase of the beat between P_{S12} and P_{S23} was calculated as $t_{S123} = 2059.686$. Herein, we ignore that the phases for the conjunction of Jupiter and Saturn vary by a few months from the average because the orbits are elliptic, which could imply a variation up to a few years of the time phases of the beat functions.

The proposed three-frequency harmonic model is then given by the function

$$\sum_{i=1}^3 h_i(t) = \sum_{i=1}^3 A_{Si} \cos \left(2\pi \frac{t - t_{Si}}{P_{Si}} \right). \quad (19)$$

The components and the beat functions generated by the model are given by the equations

$$h_1(t) = 0.83 \cos \left(2\pi \frac{t - 2000.475}{9.929656} \right), \quad (20)$$

$$h_2(t) = 1.0 \cos \left(2\pi \frac{t - 2002.364}{10.87} \right), \quad (21)$$

$$h_3(t) = 0.55 \cos \left(2\pi \frac{t - 1999.381}{11.862242} \right). \quad (22)$$

Thus, the final model becomes

$$h_{123}(t) = h_1(t) + h_2(t) + h_3(t). \quad (23)$$

To emphasize its beats we can also write

$$f_{123}(t) = \begin{cases} h_{123}(t) & \text{if } h_{123}(t) \geq 0 \\ 0 & \text{if } h_{123}(t) < 0 \end{cases} \quad (24)$$

The resulting envelope functions of the beats are

$$b_{12}(t) = 0.60 \cos \left(2\pi \frac{t - 1980.528}{114.783} \right) \quad (25)$$

$$b_{13}(t) = 0.40 \cos \left(2\pi \frac{t - 2067.044}{60.9484} \right) \quad (26)$$

$$b_{23}(t) = 0.45 \cos \left(2\pi \frac{t - 2035.043}{129.951} \right) \quad (27)$$

Figure 5 shows the three-frequency solar model of Eq. 24 (red). Figure 5A compares it against two reconstructions of the solar activity based on ^{10}Be and ^{14}C cosmogenic isotopes (blue and black, respectively) (Bard et al., 2000; Steinhilber et al., 2009). The millennial beat cycle is represented by the green curve. The model correctly hindcast all solar multi-decadal grand minima observed during the last 1000 years, known as the Oort, Wolf, Spörer, Maunder and Dalton grand solar minima. They approximately occurred when the three harmonics interfered destructively. Instead, the multi-decadal grand maxima occurred when the three harmonics interfere constructively generating a larger perturbation on the Sun.

Figure 5B compares Eq. 24 against the Northern Hemisphere proxy temperature reconstruction of Ljungqvist (2010) (black). We notice the good time-matching between the oscillations of the model and the temperature record of both the millennial and the 115-year modulations, which is better highlighted by the smoothed filtered curves at the bottom of the figure. The Roman Warm Period (RWP), Dark Age Cold Period (DACP), Medieval Warm Period (MWP), Little Ice Age (LIA) and the Current Warm Period (CWP) are well hindcast by the three-frequency Jupiter-Saturn model.

Figure 5C shows the millennial oscillation (blue) predicted by Eq. 24 given by

$$g_m(t) = \cos \left(2\pi \frac{t - 2059.686}{983.401} \right). \quad (28)$$

The curve is well correlated with the quasi millennial solar oscillation – known as the Eddy oscillation – throughout the Holocene as revealed by the ^{14}C cosmogenic isotope record (red) and other geological records (Kerr, 2001; Scafetta, 2012a, 2014b; Steinhilber et al., 2009).

Scafetta (2012a) discussed other properties of the three-frequency solar model. For example, five 59-63 year cycles appear in the period 1850-2150, which are also well correlated with the global surface temperature maxima around about 1880, 1940 and 2000. The model also predicts a grand solar minimum around the 2030s constrained between two grand solar maxima around 2000 and 2060. The modeled solar minimum around

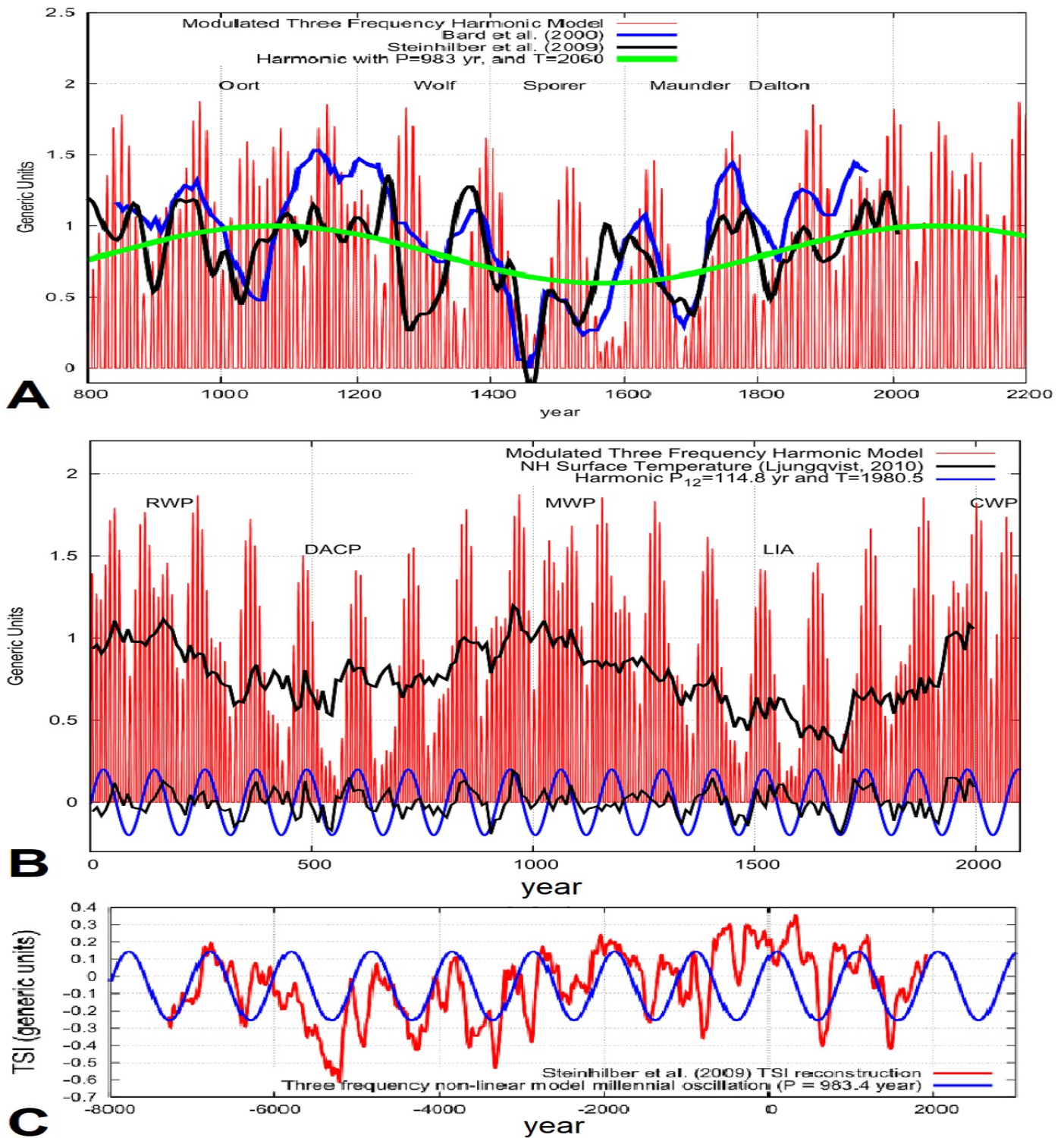


Figure 5: [A] Eq. 40 (red) against two reconstructions of solar activity based on ^{10}Be and ^{14}C cosmogenic isotopes (Bard et al., 2000; Steinhilber et al., 2009). [B]. Eq. 40 (red) against a Northern Hemisphere proxy temperature reconstruction by Ljungqvist (2010). [C] The millennial oscillation predicted by the three-frequency non-linear solar model (blue) versus the TSI proxy model by Steinhilber et al. (2009) (red). (cf. Scafetta, 2012a, 2014b).

1970, the maximum around 2000 and the following solar activity decrease, which is predicted to last until the 2030s, are compatible with the multidecadal trends of the ACRIM TSI record (Willson and Mordvinov, 2003), but not with those shown by the PMOD one (Fröh-

lich, 2006) that uses TSI modified data (Scafetta et al., 2019b) and has a continuous TSI decrease since 1980. The plots of ACRIM and PMOD TSI data are shown in Figure 4F and have been extensively commented by Scafetta et al. (2019b). Finally, the model also repro-

duces a rather long Schwabe solar cycle of about 15 years between 1680 and 1700. This long cycle was actually observed both in the $\delta^{18}\text{O}$ isotopic concentrations found in Japanese tree rings (a proxy for temperature changes) and in ^{14}C records (a proxy for solar activity) (Yamaguchia et al., 2010).

Scafetta (2014b) also suggested that the input of the planetary forcing could be nonlinearly processed by the internal solar dynamo mechanisms. As a consequence, the output function might be characterized by additional multi-decadal and secular harmonics. The main two frequency clusters are predicted at 57, 61, 65 years and at 103, 115, 130, and 150 years. These harmonics actually appear in the power spectra of solar activity (Ogurtsov et al., 2002). In particular, Cauquoin et al. (2014) found the four secular periods (103, 115, 130, 150 years) in the ^{10}Be record of 325–336 kyr ago. These authors claimed that their analyzed records do not show any evidence of a planetary influence but they did not realize that their found oscillations could be derived from the beating among the harmonics of Jupiter and Saturn with the 11-year solar cycle, as demonstrated in Scafetta (2014b).

We notice that the multi-secular and millennial hindcasts of the solar activity records made by the three-frequency Jupiter-Saturn model shown in Figure 5 are impressive because the frequencies, phases and amplitudes of the model are theoretically deduced from the orbits of Jupiter and Saturn and empirically obtained from the sunspot record from 1750 to 2010. The prolonged periods of high and low solar activity derive from the constructive and destructive interference of the three harmonics.

7 Orbital invariant inequality model: the Jovian planets and the long solar and climatic cycles

The orbital invariant inequality model was first proposed by Scafetta et al. (2016) and successively developed by Scafetta (2020) using only the orbital periods of the four Jovian planets (Table 1). It successfully reconstructs the main solar multi-decadal to millennial oscillations like those observed at 55-65 years, 80-100 years (Gleissberg cycle), 155-185 years (Jose cycle), 190-240 years (Suess-de Vries cycle), 800-1200 years (Eddy cycle) and at 2100-2500 years (Bray-Hallstatt cycle) (Abreu et al., 2012; McCracken et al., 2001, 2013; Scafetta, 2016). The model predictions well agree with the solar and climate long-term oscillations discussed, for example, in Neff et al. (2001) and McCracken et al. (2013). Let us now describe the invariant inequality model in some detail.

Given two harmonics with period P_1 and P_2 and two integers n_1 and n_2 , there is a resonance if $P_1/P_2 =$

n_1/n_2 . In the real planetary motions, this identity is almost always not satisfied. Consequently, it is possible to define a new frequency f and period P using the following equation

$$f = \frac{1}{P} = \left| \frac{n_1}{P_1} - \frac{n_2}{P_2} \right|, \quad (29)$$

which is called “inequality”. Clearly, f and P represent the beat frequency and the beat period between n_1/P_1 and n_2/P_2 . The simplest case is when $n_1 = n_2 = 1$, which corresponds to the synodal period between two planets defined in Eq. 2, which is reported below for convenience:

$$P_{12} = \frac{1}{f_{12}} = \left| \frac{1}{P_1} - \frac{1}{P_2} \right|^{-1}. \quad (30)$$

Eq. 30 indicates the average time interval between two consecutive planetary conjunctions relative to the Sun. The conjunction periods among the four Jovian planets are reported in Table 5.

Eq. 29 can be further generalized for a system of n orbiting bodies with periods P_i ($i = 1, 2, \dots, n$). This defines a generic inequality, represented by the vector (a_1, a_2, \dots, a_n) , as

$$f = \frac{1}{P} = \left| \sum_{i=1}^n \frac{a_i}{P_i} \right|, \quad (31)$$

where a_i are positive or negative integers.

Among all the possible orbital inequalities given by Eq. 31, there exists a small subset of them that is characterized by the condition:

$$\sum_{i=1}^n a_i = 0. \quad (32)$$

This special subset of frequencies is made of the synodal planetary periods (Eq. 30) and all the beats among them.

It is easy to verify that the condition imposed by Eq. 32 has a very important physical meaning: it defines a set of harmonics that are invariant with respect to any rotating system such as the Sun and the heliosphere. Given a reference system at the center of the Sun and rotating with period P_o , the orbital periods, or frequencies, seen relative to it are given by

$$f'_i = \frac{1}{P'_i} = \frac{1}{P_i} - \frac{1}{P_o}. \quad (33)$$

With respect to this rotating frame of reference, the orbital inequalities among more planets are given by:

$$f' = \frac{1}{P'} = \left| \sum_{i=1}^n \frac{a_i}{P'_i} \right| = \left| \sum_{i=1}^n \frac{a_i}{P_i} - \frac{\sum_{i=1}^n a_i}{P_o} \right|. \quad (34)$$

If the condition of Eq. 32 is imposed, we have that $f' = f$ and $P' = P$. Therefore, this specific set of orbital inequalities remains invariant regardless of the rotating frame of reference from which they are observed.

	Inv. Ineq.	Period (year)	Julian Date	Date	Long.
Jup-Sat	(1,-1,0,0)	19.8593	2451718.4	2000.4761	52° 01'
Jup-Ura	(1,0,-1,0)	13.8125	2450535.8	1997.2383	305° 22'
Jup-Nep	(1,0,0,-1)	12.7823	2450442.1	1996.9818	297° 21'
Sat-Ura	(0,1,-1,0)	45.3636	2447322.1	1988.4397	269° 05'
Sat-Nep	(0,1,0,-1)	35.8697	2447725.6	1989.5444	281° 14'
Ura-Nep	(0,0,1,-1)	171.393	2449098.1	1993.3021	289° 22'

Table 5: Heliocentric synodic invariant inequalities and periods with the timing of the planetary conjunctions closest to 2000 AD. (cf. Scafetta, 2020).

For example, the conjunction of two planets relative to the Sun is an event that is observed in the same way in all rotating systems centered in the Sun. Since the Sun is characterized by a differential rotation that depends on its latitude, this means that all solar regions simultaneously feel the same planetary beats, which can strongly favor the emergence of synchronized phenomena in the Sun. Due to this physical property, the orbital inequalities that fulfill the condition given by Eq. 32 were labeled as “invariant” inequalities.

Table 6 reports the orbital invariant inequalities generated by the large planets (Jupiter, Saturn, Uranus, and Neptune) up to some specific order. They are listed using the vectorial formalism:

$$f = \frac{1}{P} = (a_1, a_2, a_3, a_4), \quad (35)$$

where a_1 (for Jupiter), a_2 (for Saturn), a_3 (for Uranus) and a_4 (for Neptune) are positive or negative integers and their sum is zero (Eq. 32).

Two order indices, M and K , can also be used. M is the maximum value among $|a_i|$ and K is defined as

$$K = \frac{1}{2}(|a_1| + |a_2| + |a_3| + |a_4|). \quad (36)$$

Since for the invariant inequalities the condition of Eq. 32 must hold, K indicates the number of synodal frequencies between Jovian planet pairs producing a specific orbital invariant. For example, $K = 1$ means that the invariant inequality is made of only one synodal frequency between two planets, $K = 2$ indicates that the invariant inequality is made of two synodal frequencies, etc.

For example, the invariant inequality cycle $(1, -3, 1, 1)$ has $K = 3$ and it is the beat obtained by combining the synodal cycles of Jupiter-Saturn, Saturn-Uranus and Saturn-Neptune because it can be decomposed into three synodal cycles like $(1, -3, 1, 1) = (1, -1, 0, 0) - (0, 1, -1, 0) - (0, 1, 0, -1)$. In the same way, it is possible to decompose any other orbital invariant inequality. Hence, all the beats among the synodal cycles are invariant inequalities and can all be obtained using the periods and time phases listed in Table 5.

Table 6 lists all the invariant inequalities of the four Jovian planets up to $M = 5$. They can be collected into

clusters or groups that recall the observed solar oscillations. The same frequencies are also shown in Figures 6A and B revealing a harmonic series characterized by clusters with a base frequency of 0.00558 1/year that corresponds to the period of 179.2 years, which is known as the Jose cycle (1965) (Fairbridge and Shirley, 1987; Landscheidt, 1999).

The physical importance of the harmonics listed in Table 6 is shown in Figure 6C, which compares a solar activity reconstruction from a ^{14}C record, and the climatic reconstruction from a $\delta^{18}\text{O}$ record covering the period from 9500 to 6000 years ago (Neff et al., 2001): the two records are strongly correlated.

Figure 6D shows that the two records present numerous common frequencies that correspond to the cycles of Eddy (800–1200 years), Suess-de Vries (190–240 years), Jose (155–185 years), Gleissberg (80–100 years), the 55–65 year cluster, another cluster at 40–50 years, and some other features. Figure 6D also compares the common spectral peaks of the two records against the clusters of the invariant orbital inequalities (red bars) reported in Figure 6B and listed in Table 6. The figure shows that the orbital invariant inequality model well predicts all the principal frequencies observed in solar and climatic data throughout the Holocene.

The efficiency of the model in hindcasting both the frequencies and the phases of the observed solar cycles can also be more explicitly shown. For example, the model perfectly predicts the great Bray-Hallstatt cycle (2100–2500 years) that was studied in detail by McCracken et al. (2013) and Scafetta et al. (2016). The first step to apply the model is to determine the constituent harmonics of the invariant inequality $(1, -3, 1, 1)$. This cycle is a combination of the orbital periods of Jupiter, Saturn, Uranus and Neptune that gives

$$P_{JSUN} = \frac{1}{f_{JSUN}} = \left(\frac{1}{P_J} - \frac{3}{P_S} + \frac{1}{P_U} + \frac{1}{P_N} \right)^{-1} = 2317.56\text{yr}. \quad (37)$$

The constituent harmonics are the synodic cycles of Jupiter-Saturn, Saturn-Uranus and Saturn-Neptune as described by the following relation

$$(1, -3, 1, 1) = (1, -1, 0, 0) - (0, 1, -1, 0) - (0, 1, 0, -1). \quad (38)$$

Thus, the invariant inequality $(1, -3, 1, 1)$ is the longest beat modulation generated by the superposition of these

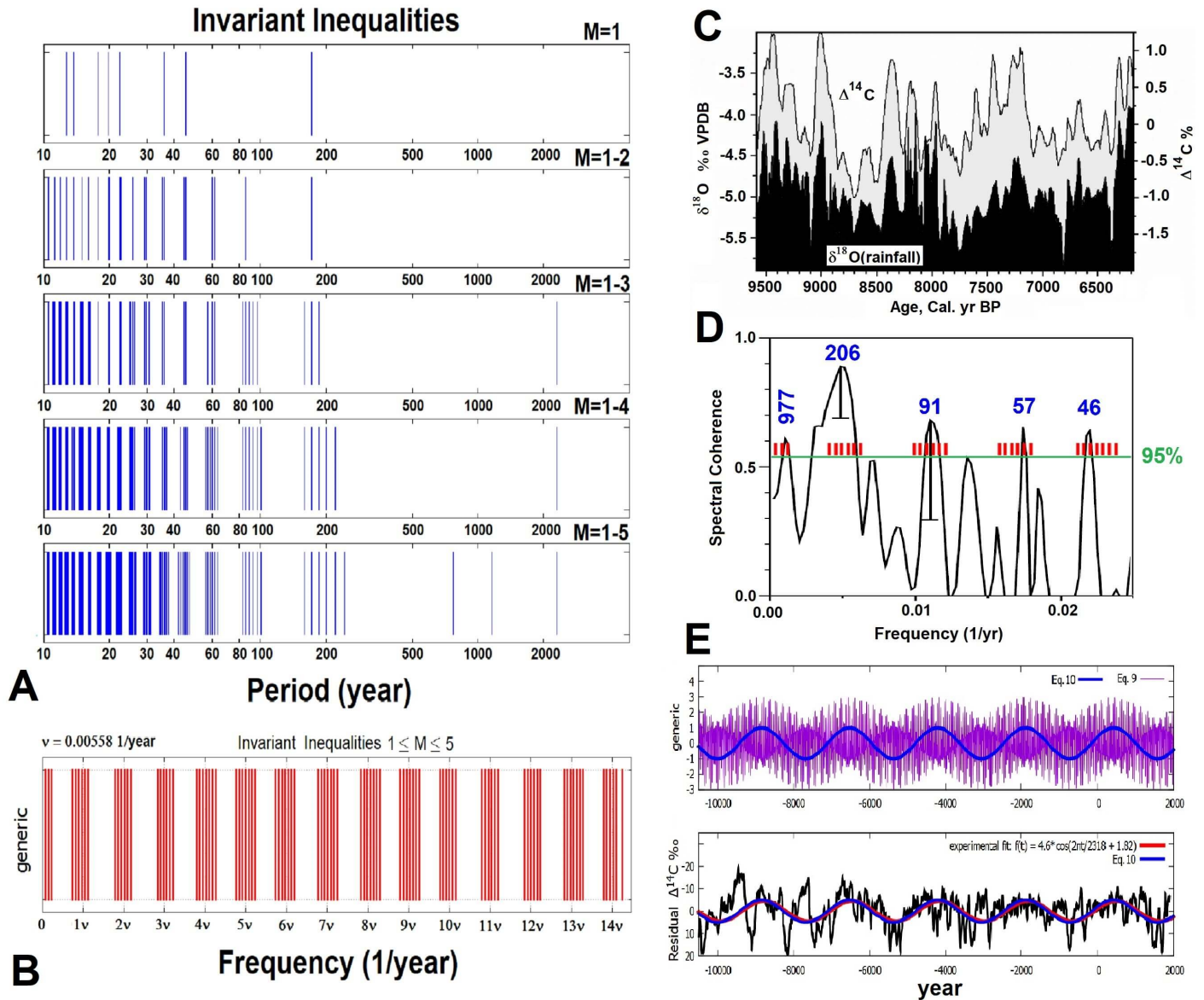


Figure 6: [A] The periods of the orbital invariant inequalities produced by Jupiter, Saturn, Uranus and Neptune for $1 \leq M \leq 5$. [B] The same harmonics highlighting their base frequency ν of the Jose cycle (179.2 years). (cf. Scafetta, 2020). [C] Visual correlation between the INTCAL98 atmospheric $\Delta^{14}C$ record (Stuiver et al., 1998) and a speleothem calcite $\delta^{18}O$ record (adapted from Neff et al., 2001). [D] Comparison between the cross-spectral analysis of the two records in C against the invariant inequalities of the solar system of Table 6 (red bars). (cf. Scafetta, 2020). [E, Top] Eqs. 39 and 40 that model the Hallstatt oscillation predicted by the invariant inequality (1, -3, 1, 1). [E, Bottom] Eq. 40 (blue) against the the $\Delta^{14}C$ record (black) throughout the Holocene (Reimer et al., 2004, IntCal04.14c) and the observed Hallstatt oscillation deduced from a regression harmonic model (red). (cf. Scafetta et al., 2016; Scafetta, 2020).

three synodic cycles and it can be expressed as the periodic function

$$f(t) = \sin\left(2\pi \frac{t-t_{JS}}{P_{JS}}\right) + \sin\left(2\pi \frac{t-t_{SU}}{P_{SU}}\right) + \sin\left(2\pi \frac{t-t_{SN}}{P_{SN}}\right) \quad (39)$$

where P_{ij} are the synodic periods and t_{ij} are the correspondent time-phases listed in Table 5.

Eq. 39 is plotted in Figure 6E and shows the long beat modulation superposed to the Bray-Hallstatt pe-

riod of 2318 years found in the $\Delta^{14}C$ (‰) record (black) throughout the Holocene (Reimer et al., 2004, IntCal04.14c). This beat cycle is captured, for example, by the function:

$$f_B(t) = -\sin\left(2\pi \frac{t-t_{JS}}{P_{JS}} - 2\pi \frac{t-t_{SU}}{P_{SU}} - 2\pi \frac{t-t_{SN}}{P_{SN}}\right), \quad (40)$$

whose period is 2318 years and the timing is fixed by the three conjunction epochs and the respective synodic

(Jup, Sat, Ura, Nep)	(M, K)	T (year)	cluster	(Ven, Ear, Jup, Sat)	(M, K)	T (year)	
(1, -3, 5, -3)	(5, 6)	42.1	~ 45 year	(3, -5, 5, -3)	(5, 8)	5.10	
(0, 0, 4, -4)	(4, 4)	42.8		(-1, 2, -3, 2)	(3, 4)	5.28	
(2, -5, 1, 2)	(5, 5)	43.7		(2, -3, -2, 3)	(3, 5)	5.43	
(-1, 3, 3, -5)	(5, 6)	43.7		(-3, 5, 2, -4)	(5, 7)	6.40	
(1, -2, 0, 1)	(2, 2)	44.5		(0, 0, 3, -3)	(3, 3)	6.62	
(0, 1, -1, 0)	(1, 1)	45.4		(3, -5, 4, -2)	(5, 7)	6.86	
(-1, 4, -2, -1)	(4, 4)	46.3		(-1, 2, -4, 3)	(4, 5)	7.19	
(1, -1, -5, 5)	(5, 6)	47.2		(2, -3, -3, 4)	(4, 6)	7.47	
(1, -3, 4, -2)	(4, 5)	55.8		(-3, 5, 1, -3)	(5, 6)	9.44	
(0, 0, 3, -3)	(3, 3)	57.1		(0, 0, 2, -2)	(2, 2)	9.93	
(2, -5, 0, 3)	(5, 5)	58.6	~ 60 year	(3, -5, 3, -1)	(5, 6)	10.47	
(-1, 3, 2, -4)	(4, 5)	58.6		(-1, 2, -5, 4)	(5, 6)	11.27	
(1, -2, -1, 2)	(2, 3)	60.1		(2, -3, -4, 5)	(5, 7)	11.97	
(0, 1, -2, 1)	(2, 2)	61.7		(-3, 5, 0, -2)	(5, 5)	18.00	
(-1, 4, -3, 0)	(4, 4)	63.4		(0, 0, 1, -1)	(1, 1)	19.86	
(1, -3, 3, -1)	(3, 4)	82.6		(3, -5, 2, 0)	(5, 5)	22.14	
(0, 0, 2, -2)	(2, 2)	85.7		(-3, 5, -1, -1)	(5, 5)	192.8	
(2, -5, -1, 4)	(5, 6)	89.0		Gleissberg			
(-1, 3, 1, -3)	(3, 4)	89.0					
(1, -2, -2, 3)	(3, 4)	92.5					
(0, 1, -3, 2)	(3, 3)	96.4					
(-1, 4, -4, 1)	(4, 5)	100.6					
(1, -3, 2, 0)	(3, 3)	159.6					
(0, 0, 1, -1)	(1, 1)	171.4	Jose		(-2, 3, 4, -5)	(5, 7)	6.63
(2, -5, -2, 5)	(5, 7)	185.1			(2, -4, -2, 4)	(4, 6)	7.18
(-1, 3, 0, -2)	(3, 3)	185.1	Suess-de Vries		(1, -2, -1, 2)	(2, 3)	14.35
(1, -2, -3, 4)	(4, 5)	201.1			(3, -5, 2, 0)	(5, 5)	22.14
(0, 1, -4, 3)	(4, 4)	220.2	Eddy	(1, -5, 4, 0)	(5, 5)	40.82	
(-1, 4, -5, 2)	(5, 6)	243.4					
(0, -1, 5, -4)	(5, 5)	772.7	Bray-Hallstatt				
(-1, 2, 4, -5)	(5, 6)	1159					
(1, -3, 1, 1)	(3, 3)	2318					

Table 6: (Left) List of invariant inequalities for periods $T \geq 40$ years and $M \leq 5$ for Jupiter, Saturn, Uranus, Neptune. (Right) The same for Venus, Earth, Jupiter, and Saturn, and for Mercury, Venus, Earth and Jupiter. (cf. Scafetta, 2020).

periods. In fact, the argument of the above sinusoidal function is the sum of three terms that correspond to those of Equation 38. Equation 40 is plotted in Figure 6E as the blue curve.

Three important invariant inequalities – $(1, -3, 2, 0)$, $(0, 0, 1, -1)$ and $(-1, 3, 0, -2)$ – are found within the Jose 155–185 year period band:

$$P_{JSU} = \frac{1}{f_{JSU}} = \left(\frac{1}{P_J} - \frac{3}{P_S} + \frac{2}{P_U} \right)^{-1} = 159.59 \text{ yr}, \quad (41)$$

$$P_{UN} = \frac{1}{f_{UN}} = \left(\frac{1}{P_U} - \frac{1}{P_N} \right)^{-1} = 171.39 \text{ yr}, \quad (42)$$

$$P_{JSN} = \frac{1}{f_{JSN}} = \left(-\frac{1}{P_J} + \frac{3}{P_S} - \frac{2}{P_N} \right)^{-1} = 185.08 \text{ yr}. \quad (43)$$

The long beat between Eq. 42 and Eq. 41 – that is $(0, 0, 1, -1) - (-1, 3, 0, -2) = (1, -3, 1, -1)$ – is the great Bray–Hallstatt cycle. The fast beat between Eq. 42 and Eq. 43 – $(0, 0, 1, -1) + (-1, 3, 0, -2) = (-1, 3, 1, -3)$ – is the Gleissberg 89-year cycle, which also corresponds to half of the Jose period of ~ 178 year that regulates the harmonic structure of the wobbling of the solar motion.

Another interesting invariant inequality is $(1, -2, -1, 2) = (1, 0, -1, 0) - 2(0, 1, 0, -1)$, which is a beat between the synodic period of Jupiter and Uranus $(1, 0, -1, 0)$ and the first harmonic of the synodic period of Saturn and Neptune. The period is:

$$P_{JSN} = \frac{1}{f_{JSN}} = \left(\frac{1}{P_J} - \frac{2}{P_S} - \frac{1}{P_U} + \frac{2}{P_N} \right)^{-1} = 60.1 \text{ yr}, \quad (44)$$

The beat oscillation is given by the equation:

$$f(t) = \cos\left(2\pi \frac{t - t_{JU}}{P_{JU}}\right) + \cos\left(2\pi \cdot 2 \frac{t - t_{SN}}{P_{SN}}\right), \quad (45)$$

that shows a 60.1-year beat oscillation. The pattern is found in both solar and climate records and could be physically relevant because the maxima of the 60-year beat occur during specific periods – the 1880s, 1940s, and 2000s – that were characterized by maxima in climatic records of global surface temperatures and in several other climate index records (Agnihotri and Dutta, 2003; Scafetta, 2013, 2014c; Wyatt and Curry, 2014). The 60-year oscillation was even found in the records of the historical meteorite falls in China from AD 619 to 1943 (Chang and Yu, 1981; Scafetta et al., 2019a; Yu et al., 1983).

An astronomical 60-year oscillation can be obtained in several ways. In particular, Scafetta (2010) and (2012c) showed that it is also generated by three consecutive conjunctions of Jupiter and Saturn since their synodic cycle is 19.86 years and every three alignments the conjunctions occur nearly in the same constellation. The three consecutive conjunctions are different from each other because of the ellipticity of the orbits. The 60-year pattern has been known since antiquity as the Trigon of the Great Conjunctions (Kepler, 1606), which also slowly rotates generating a quasi-millennial cycle known as the Great Inequality of Jupiter and Saturn (Etz, 2000; Lovett, 1895; Scafetta, 2012c; Wilson, 2013).

Both the 60-year and the quasi-millennial oscillations also characterize the evolution of the instantaneous eccentricity function of Jupiter (Scafetta et al., 2019a). The quasi millennial oscillation (the Hedy cycle) could be related to the two orbital invariant inequalities $(0, -1, 5, -4) \equiv 772.7$ years and $(-1, 2, 4, -5) \equiv 1159$ years. Their beat frequency being $(0, -1, 5, -4) - (-1, 2, 4, -5) = (1, -3, 1, 1) \equiv 2318$ years, which corresponds to the Bray–Hallstatt cycle. Their mean frequency, instead, is $0.5(0, -1, 5, -4) + 0.5(-1, 2, 4, -5) = 0.5(-1, 1, 9, -9) \equiv 927$ years that reminds the Great Inequality cycle of Jupiter and Saturn suggesting that this great cycle could also be generated by the beat between the synodic period of Jupiter and Saturn, $(1, -1, 0, 0)$ and the ninth harmonic of the synodic period of Uranus and Neptune, $9(0, 0, 1, -1)$.

The invariant inequality model can be extended to all the planets of the solar system (see Tables 3 and 4 and 6). The ordering of the frequencies according to their physical relevance depends on the specific physical function involved (e.g. tidal forcing, angular momentum transfer, space weather modulation, etc.) and will be addressed in future work.

8 The Suess-de Vries cycle (190-240 years)

The Suess-de Vries cycle is an important secular solar oscillation commonly found in radiocarbon records (de

Vries, 1958; Suess, 1965). Several recent studies have highlighted its importance (Abreu et al., 2012; Beer et al., 2018; Lüdecke et al., 2015; McCracken et al., 2013; Neff et al., 2001; Stefani et al., 2020b, 2021; Wagner et al., 2001; Weiss and Tobias, 2016). Its period varies between 200 and 215 years but the literature also suggests a range between 190 and 240 years.

Stefani et al. (2021) argued that the Suess-de Vries cycle, together with the Hale and the Gleissberg-type cycles, could emerge from the synchronization between the 11.07-year periodic tidal forcing of the Venus–Earth–Jupiter system and the 19.86-year periodic motion of the Sun around the barycenter of the solar system due to Jupiter and Saturn. This model yields a Suess-de Vries-type cycle of 193 years.

Actually, the 193-year period is the orbital invariant inequality $(-3, 5, -1, -1) = (0, 0, 1, -1) - (3, -5, 2, 0)$ where $(0, 0, 1, -1)$ is the synodic cycle of Jupiter and Saturn (19.86 years) and $(3, -5, 2, 0)$ is the 22.14-year orbital inequality cycle of Venus, Earth and Jupiter (Eq. 5). We also notice that $(0, 0, 1, -1) + (3, -5, 2, 0) = (3, -5, 3, -1)$ corresponds to the period of 10.47 years which is a periodicity that has been observed in astronomical and climate records (Scafetta, 2014b; Scafetta et al., 2020).

The orbital invariant inequality model discussed in Section 7 provides an alternative and/or complementary origin of the Suess-de Vries cycle. In fact, the orbital invariant inequalities among Jupiter, Saturn, Uranus and Neptune form a cluster of planetary beats with periods between 200 and 240 years. Thus, the Suess-de Vries cycle might also emerge as beat cycles among the orbital invariant inequalities with periods around 60 years and those belonging to the Gleissberg frequency band with periods around 85 years. See Table 6. In fact, their synodic cycles would approximately be

$$\frac{1}{1/60 - 1/85} = 204 \text{ yr.} \quad (46)$$

It might also be speculated that the Suess-de Vries cycle originates from a beat between the Trigon of the Great Conjunctions of Jupiter and Saturn ($3 \times 19.862 = 59.6$ years, which is an oscillation that mainly emerges from the synodical cycle between Jupiter and Saturn combined with the eccentricity of the orbit of Jupiter) and the orbital period of Uranus (84 years). In this case, we would have $1/(1/59.6 - 1/84) = 205$ years.

The last two estimates coincide with the 205-year Suess-de Vries cycle found in radiocarbon records by Wagner et al. (2001) and are just slightly smaller than the 208-year cycle found in other similar recent studies (Abreu et al., 2012; Beer et al., 2018; McCracken et al., 2013; Weiss and Tobias, 2016)

We notice that the natural planetary cycles that could theoretically influence solar activity are either the orbital invariant inequality cycles (which involve the synodic cycles among the planets assumed to be moving

on circular orbits) and the orbital cycles of the planets themselves because the orbits are not circular but eccentric, and their harmonics.

9 Evidences for planetary periods in climatic records

A number of solar cycles match the periods found in climatic records (see Figures 5, 6 and 7) and often appear closely correlated for millennia (e.g.: Neff et al., 2001; Scafetta et al., 2004, 2006; Scafetta, 2009, 2021; Steinhilber et al., 2012, and many others).

Evidences for a astronomical origin of the Sub-Milankovitch climate oscillations have been discussed in several studies (e.g.: Scafetta, 2010, 2014b, 2016, 2018, 2021). Let us now summarize the main findings relative to the global surface temperature record from 1850 to 2010.

Figures 7A and B compare the time-frequency analyses between the speed of the Sun relative to the center of mass of the solar system (Figure 2) and the HadCRUT3 global surface records (Scafetta, 2014b). It can be seen that the global surface temperature oscillations mimic several astronomical cycles at the decadal and multi-decadal scales, as first noted in Scafetta (2010) and later confirmed by advanced spectral coherence analyses (Scafetta, 2016, 2018).

The main periods found in the speed of the Sun (Figure 7A) are at about 5.93, 6.62, 7.42, 9.93, 11.86, 13.8, 20 and 60 years. Most of them are related to the orbits of Jupiter and Saturn. The main periods found in the temperature record (Figure 7B) are at about 5.93, 6.62, 7.42, 9.1, 10.4, 13.8, 20 and 60 years. Most of these periods appear to coincide with orbital invariant inequalities (Table 6) but the 9.1 and 10.4-year cycles.

Among the climate cycles, it is also found an important period of about 9.1 years, which is missing among the main planetary frequencies shown in Figure 7A. Scafetta (2010) argued that this oscillation is likely linked to a combination of the 8.85-year lunar apsidal line rotation period, the first harmonic of the 9-year Saros eclipse cycle and the 9.3-year first harmonic of the soli-lunar nodal cycle (Cionco et al., 2021; Scafetta, 2012d, supplement). These three lunar cycles induce oceanic tides with an average period of about 9.1 years (Wood, 1986; Keeling and Whorf, 2000) that could affect the climate system by modulating the atmospheric and oceanic circulation.

The 10.4-year temperature cycle is variable and appears to be the signature of the 11-year solar cycle that varies between the Jupiter-Saturn spring tidal cycle (9.93 years) and the orbital period of Jupiter (11.86 years). Note that in Figure 7B, the frequency of this temperature signal increased in time from 1900 to 2000. This agrees with the solar cycle being slightly longer (and smaller) at the beginning of the 20th century and shorter (and larger) at its end (see Figure 3). We also

notice that the 10.46-year period corresponds to the orbital invariant inequality $(3, -5, 3, -1)$ among Venus, Earth, Jupiter and Saturn.

The above findings were crucial for the construction of a semi-empirical climate model based on the several astronomically identified cycles (Scafetta, 2010, 2013). The model included the 9.1-year solar-lunar cycle, the astronomical-solar cycles at 10.5, 20, 60 and, in addition, two longer cycles with periods of 115 years (using Eq. 25) and a millennial cycle here characterized by an asymmetric 981-year cycle with a minimum around 1700 (the Maunder Minimum) and two maxima in 1080 and 2060 (using Eq. 28). The model was completed by adding the volcano and the anthropogenic components deduced from the ensemble average prediction of the CMIP5 global circulation models assuming an equilibrium climate sensitivity (ECS) of about 1.5°C that is half of that of the model average, which is about 3°C. This operation was necessary because the identified natural oscillations already account for at least 50% of the warming observed from 1970 to 2000. Recently, Scafetta (2021) upgraded the model by adding some higher frequency cycles.

Figure 7C shows the HadCRUT4.6 global surface temperature record (Morice et al., 2012) against the ensemble average simulations produced by the CMIP6 global circulation models (GCMs) using historical forcings (1850-2014) extended with three different shared socioeconomic pathway (SSP) scenarios (2015-2100) (Eyring et al., 2016). Figure 7D shows the same temperature record against the proposed semi-empirical astronomical harmonic model under the same forcing conditions. The comparison between panels C and D shows that the semi-empirical harmonic model performs significantly better than the classical GCMs in hindcasting the 1850-2020 temperature record. It also predicts moderate warming for the future decades, as explained in detail by Scafetta (2013, 2021).

10 Possible physical mechanisms

Many authors suggest that solar cycles revealed in sunspot and cosmogenic records could derive from a deterministic non-linear chaotic dynamo (Weiss and Tobias, 2016; Charbonneau, 2020, 2022). However, the assumption that solar activity is only regulated by dynamical and stochastic processes inside the Sun has never been validated mainly because these models have a poor hindcasting capability.

We have seen how the several main planetary harmonics and orbital invariant inequalities tend to cluster towards specific frequencies that characterize the observed solar activity cycles. This suggests that the strong synchronization among the planetary orbits could be further extended to the physical processes that are responsible for the observed solar variability.

The physical mechanisms that could explain how the planets may directly or indirectly influence the Sun are

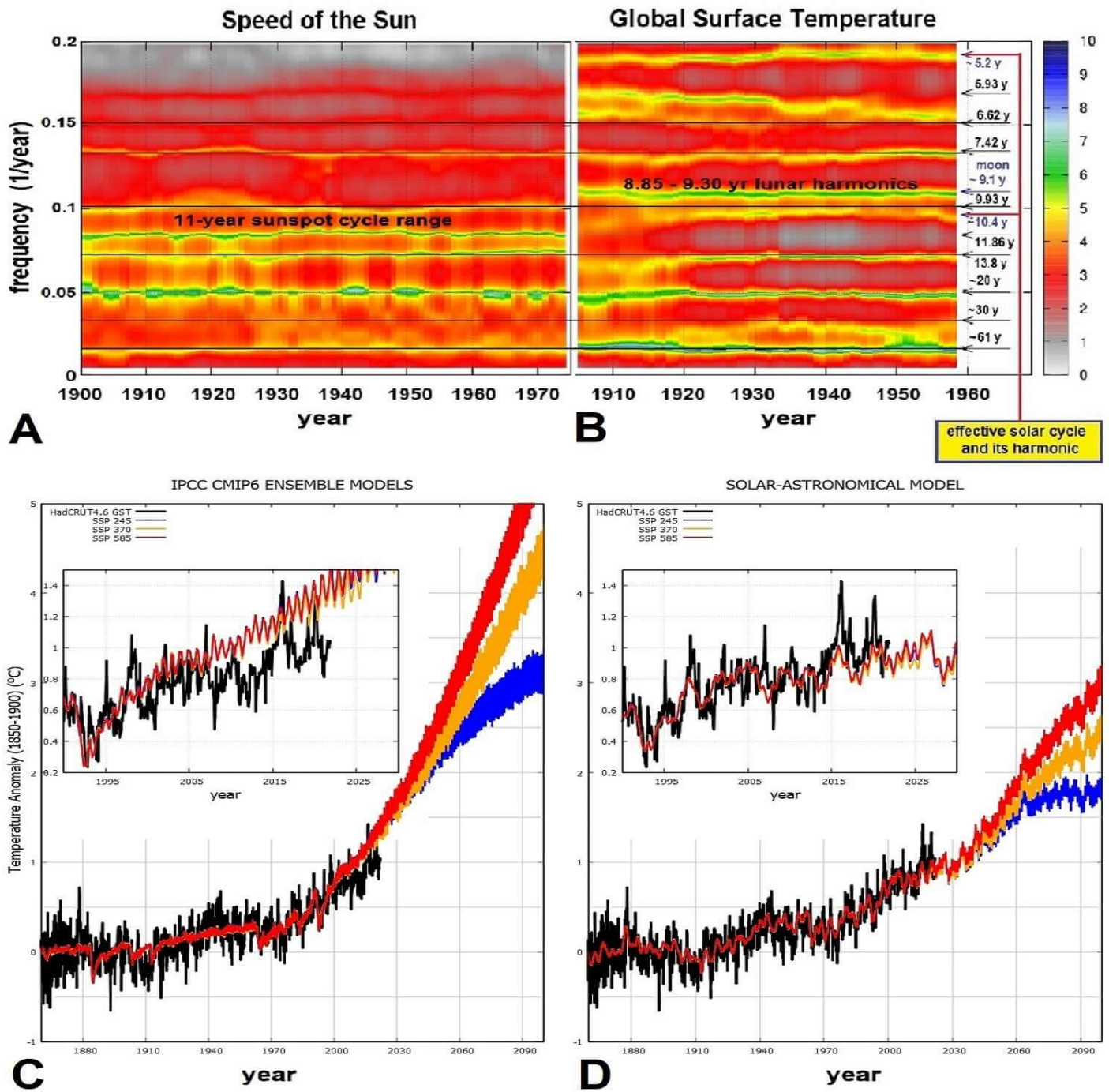


Figure 7: [A] Time-frequency analysis ($L = 110$ years) of the speed of the Sun relative to the barycenter of the solar system. [B] Time frequency analysis ($L = 110$ years) of the detrended HadCRUT3 temperature record. (cf. Scafetta, 2014b). [C] Ensemble CMIP6 GCM mean simulations for different emission scenarios versus the HadCRUT global surface temperatures. [D] The same record compared with the solar-astronomical harmonic climate model Scafetta (2013) updated in Scafetta (2021).

currently unclear. It can be conjectured that the solar dynamo might have been synchronized to some planetary periods under the action of harmonic forcings acting on it for several hundred million or even billion years. In fact, as pointed out by Huygens in the 17th century, synchronization can occur even if the harmonic forcing is very weak but lasts long enough (Pikovsky et

al., 2001).

There may be two basic types of mechanisms referred to how and where in the Sun the planetary forcing is acting. In particular, we distinguish between the mechanisms that interact with the outer regions of the Sun and those that act in its interior.

1. Planetary tides can perturb the surface magnetic activity of the Sun, the solar corona, and thus the solar wind. The solar wind, driven by the rotating twisted magnetic field lines (Parker, 1958; Tattersall, 2013), can reconnect with the magnetic fields of the planets when they get closer during conjunctions. This would modulate the solar magnetic wind density distribution and the screening efficiency of the whole heliosphere on the incoming cosmic rays. The effect would be a modulation of the cosmogenic records which then also act on the cloud cover. It is also possible that the planets can focus and modulate by gravitational lensing the flux of interstellar and interplanetary matter – perhaps even of dark matter – towards the Sun and the Earth stimulating solar activity (Bertolucci et al., 2017; Scafetta, 2020; Zioutas et al., 2022) and, again, contributing to clouds formation on Earth which alters the climate.
2. Gravitational planetary tides and torques could reach the interior of the Sun and synchronize the solar dynamo by forcing its tachocline (Abreu et al., 2012; Stefani et al., 2016, 2019, 2021) or even modulate the nuclear activity in the core (Scafetta, 2012b; Wolff and Patrone, 2010).

Scafetta and Willson (2013b) argued that these two basic mechanisms could well complement each other. In principle, it might also be possible that the physical solar dynamo is characterized by a number of natural frequencies that could resonate with the external periodic forcings yielding some type of synchronization. Let us briefly analyze several cases.

10.1 Mechanisms associated with planetary alignments

The frequencies associated with planetary alignments and, in particular, those of the Jovian planets, were found to reproduce the main observed cycles in solar and climatic data. Scafetta (2020) showed examples of gravitational field configurations produced by a toy-model made of four equal masses orbiting around a 10 times more massive central body.

The Sun could feel planetary conjunctions because at least twenty-five out of thirty-eight largest solar flares were observed to start when one or more planets among Mercury, Venus, Earth, and Jupiter were either nearly above the position of the flare (within 10° longitude) or on the opposite side of the Sun (Hung, 2007). For example, Mörner et al. (2015) showed that, on January 7 2014, a giant solar flare of class X1.2 was emitted from the giant sunspot active region AR1944 (NASA, 2014), and that the flare pointed directly toward the Earth when Venus, Earth and Jupiter were exactly aligned in a triple conjunction and the planetary tidal index calculated by Scafetta (2012b) peaked at the same time.

Hung (2007) estimated that the probability for this to happen at random was 0.039%, and concluded that “*the force or momentum balance (between the solar atmospheric pressure, the gravity field, and magnetic field) on plasma in the looping magnetic field lines in solar corona could be disturbed by tides, resulting in magnetic field reconnection, solar flares, and solar storms.*” Comparable results and confirmations that solar flares could be linked to planetary alignments were recently discussed in Bertolucci et al. (2017) and Petrakou (2021).

10.2 Mechanisms associated with the solar wobbling

The movement of the planets and, in particular, of the Jovian ones, are reflected in the solar wobbling. Charvátová (2000) and Charvátová and Hejda (2014) showed that the solar wobbling around the center of mass of the solar system forms two kinds of complex trajectories: an ordered one, where the orbits appear more symmetric and circular, and a disordered type, where the orbits appear more eccentric and randomly distributed. These authors found that the alternation between these two states presents periodicities related, for example, to the Jose (~ 178 years) and Bray–Hallstatt (~ 2300 years) cycles.

Figure 8A compares the Bray–Hallstatt cycle found in the $\Delta^{14}C$ (‰) record (black) throughout the Holocene (Reimer et al., 2004, IntCal04.14c) with two orbital records representing the periods of the pericycle and apocycle orbital arcs of the solar trajectories as extensively discussed by Scafetta et al. (2016). Figure 8B shows the solar wobbling for about 6000 years where the alternation of ordered and disordered orbital patterns typically occurs according to the Bray–Hallstatt cycle of 2318 years (Scafetta et al., 2016).

In particular, the astronomical records show that the Jose cycle is modulated by the Bray–Hallstatt cycle. Figures 8C and D show examples of how planetary configurations can reproduce the Bray–Hallstatt cycle: see details in Scafetta et al. (2016). The fast oscillations correspond to the orbital invariant inequalities with periods of 159, 171.4 and 185 years while the long beat oscillation corresponds to the orbital invariant inequality with a period of 2318 years, which perfectly fits the Bray–Hallstatt cycle as estimated in McCracken et al. (2013) (see Table 6). It is possible that the pulsing dynamics of the heliosphere can periodically modulate the solar wind termination shock layer and, therefore, the incoming interstellar dust and cosmic ray fluxes.

10.3 Mechanisms associated with planetary tides and tidal torques

Discussing the tidal interactions between early-type binaries, Goldreich and Nicholson (1989) demonstrated that the tidal action and torques can produce important effects in the thin overshooting region between the

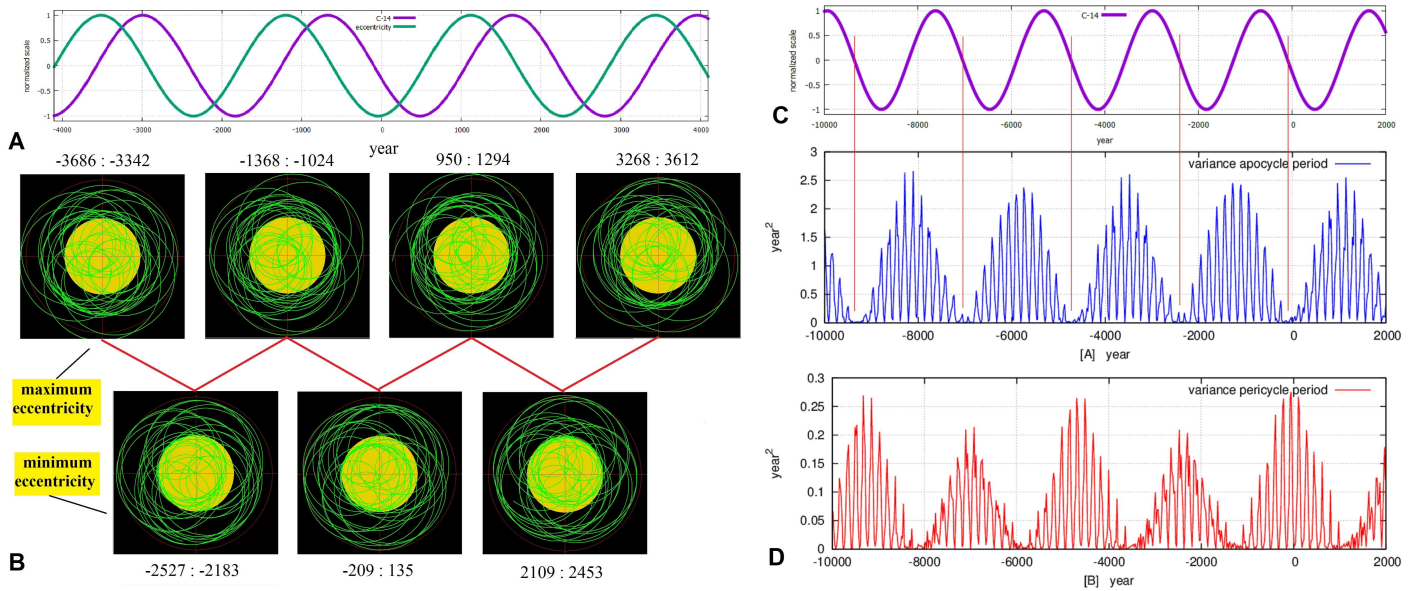


Figure 8: [A] The Hallstatt oscillation (2318 years) found in $\Delta^{14}\text{C}$ (‰) record and in the eccentricity function of the barycenter of the planets relative to the Sun. [B] Ordered and disordered orbits of the barycenter of the planets relative to the Sun. [C and D] The Hallstatt oscillation found in $\Delta^{14}\text{C}$ (‰) record and in the apocycles and pericycles of the orbits of the center of mass of the planets relative to the Sun. (cf. Scafetta et al., 2016).

radiative and the convective zone, which is very close to the tachocline. This would translate both in tidal torques and in the onset of g-waves moving throughout the radiative region. A similar mechanism should also take place in late-type stars like the Sun (Goodman and Dickson, 1998).

Abreu et al. (2012) found an excellent agreement between the long-term solar cycles and the periodicities in the planetary tidal torques. These authors assumed that the solar interior is characterized by a non-spherical tachocline. Under such a condition, the planetary gravitational forces exert a torque on the tachocline itself that would then vary with the distribution of the planets around the Sun. These authors showed that the torque function is characterized by some specific planetary frequencies that match those observed in cosmogenic radionuclide proxies of solar activity. The authors highlighted spectral coherence at the following periods: 88, 104, 150, 208 and 506 years. The first four periods were discussed above using alternative planetary functions; the last period could be a harmonic of the millennial solar cycle also discussed above and found in the same solar record (Scafetta, 2012a, 2014b).

Abreu et al. (2012) observed that the tachocline approximately coincides with the layer at the bottom of the convection zone where the storage and amplification of the magnetic flux tubes occur. These are the flux tubes that eventually erupt at the solar photosphere to form active regions. The tachocline layer is in a critical state because it is very sensitive to small perturbations being between the radiative zone characterized by stable stratification ($\delta < 0$) and the convective zone characterized by unstable stratification ($\delta > 0$). The proposed

hypothesis is that the planetary tides could influence the magnetic storage capacity of the tachocline region by modifying its entropy stratification and the superadiabaticity parameter δ , thereby altering the maximum field strength of the magnetic flux tubes that regulate the solar dynamo.

However, Abreu et al. (2012) also acknowledged that their hypothesis could not explain how the tiny tidal modification of the entropy stratification could produce an observable effect although they conjectured the presence of a resonance mediated by gravity waves.

The planetary tidal influence on the solar dynamo has been rather controversial because the tidal accelerations at the tachocline layer are about 1000 times smaller than the accelerations of the convective cells (Jager and Versteegh, 2005). Scafetta (2012b) calculated that the gravitational tidal amplitudes produced by all the planets on the solar chromosphere are of the order of one millimeter or smaller (see Table 7). More recently, Charbonneau (2022) critiqued Stefani et al. (2019, 2021) by observing that also the planetary tidal forcings of Jupiter and Venus could only exert a “homeopathic” influence on the solar tachocline concluding that they should be unable to synchronize the dynamo. Charbonneau (2022) also observed that even angular momentum transport by convective overshoot into the tachocline would be inefficient and concluded that synchronization could only be readily achieved in presence of high forcing amplitudes, stressing the critical need for a powerful amplification mechanism.

While it is certainly true that the precise underlying mechanism is not completely understood, the rough energetic estimate that 1 mm tidal height corresponds

	mass (kg)	semi-major axis (m)	perihelion (m)	aphelion (m)	mean tidal elong. (m)	diff. tidal elong. (m)	Sun rot. (days)
Me	3.30E23	5.79E10	4.60E10	6.98E10	3.0E-4 (7.5E-4)	4.3E-4 (1.1E-3)	37.92
Ve	4.87E24	1.08E11	1.08E11	1.09E11	6.8E-4 (1.7E-3)	2.6E-5 (6.6E-5)	30.04
Ea	5.97E24	1.50E11	1.47E11	1.52E11	3.2E-4 (7.9E-4)	3.2E-5 (7.9E-5)	28.57
Ma	6.42E23	2.28E11	2.07E11	2.49E11	9.6E-6 (2.4E-5)	5.5E-6 (1.4E-5)	27.56
Ju	1.90E27	7.79E11	7.41E11	8.17E11	7.1E-4 (1.8E-3)	2.1E-4 (5.2E-4)	26.66
Sa	5.69E26	1.43E12	1.35E12	1.51E12	3.4E-5 (8.5E-5)	1.2E-5 (2.9E-5)	26.57
Ur	8.68E25	2.88E12	2.75E12	3.00E12	6.4E-7 (1.6E-6)	1.7E-7 (4.3E-7)	26.52
Ne	1.02E26	4.50E12	4.45E12	4.55E12	2.0E-7 (5.0E-7)	1.3E-8 (3.3E-8)	26.51

Table 7: Mean tidal elongations at the solar surface produced by all planets. “Diff. tidal elongation” is the difference between the tides at perihelion and aphelion. The 26.5-day mean solar rotation as seen by the planets. Tidal elongations are calculated for Love-number 3/2 and 15/4, the latter being inside parentheses. (cf. Scafetta, 2012b).

to 1 m/s velocity at the tachocline level might still entail sufficient capacity for synchronization by changing the (sensitive) field storage capacity (Abreu et al., 2012) or by synchronizing that part of α that is connected with the Tayler instability or by the onset of magneto-Rossby waves at the tachocline (Dikpati et al., 2017; Zakharashvili, 2018). In all cases, it could be possible that only a few high-frequency planetary forcing (e.g. the 11.07-year Venus-Earth-Jupiter tidal model) are able to efficiently synchronize the solar dynamo (Stefani et al., 2016; Stefani, 2018; Stefani et al., 2019). At the same time, additional and longer solar cycles could emerge when some feature of the dynamo is also modulated by the angular momentum exchange associated with the solar wobbling (Stefani et al., 2021). Finally, Albert et al. (2021) proposed that stochastic resonance could explain the multi-secular variability of the Schwabe cycle by letting the dynamo switch between two distinct operating modes as the solution moves back and forth from the attraction basin of one to the other.

Alternatively, the problem of the tidal “homeopathic” influence on the tachocline could be solved by observing that tides could play some more observable role in the large solar corona where the solar wind originates, or in the wind itself at larger distances from the Sun where the tides are stronger, or even in the solar core where they could actually trigger a powerful response from nuclear fusion processes. Let us now discuss the latter hypothesis.

10.4 A possible solar amplification of the planetary tidal forcing

A possible amplification mechanism of the effects of the tidal forcing was introduced by Wolff and Patrone (2010) and Scafetta (2012b).

Wolff and Patrone (2010) proposed that tidal forcing could act inside the solar core inducing waves in the plasma by mixing the material and carrying fresh fuel to the deeper and hotter regions. This mechanism would make solar-type stars with a planetary system slightly brighter because their fuel would burn more quickly.

Scafetta (2012b) further developed this approach and introduced a physical mechanism inspired by the mass-luminosity relation of main-sequence stars. The basic idea is that the luminosity of the core of the Sun can be written as

$$L(t) \approx L_{\odot} + A \cdot \dot{\Omega}_{tidal}(t), \quad (47)$$

where L_{\odot} is the baseline luminosity of the star without planets and $\Delta L_{tidal}(t) = A \cdot \dot{\Omega}_{tidal}(t)$ is the small luminosity increase induced by planetary tides inside the Sun. $\dot{\Omega}_{tidal}(t)$ is the rate of the gravitational tidal energy which is continuously dissipated in the core and A is the amplification factor related to the triggered luminosity production via H-burning.

To calculate the magnitude of the amplification factor A we start by considering the Hertzsprung-Russell *mass-luminosity relation*, which establishes that, if the mass of a star increases, its luminosity L increases as well. In the case of a G-type main-sequence star, with luminosity L and mass $M = M_{\odot} + \Delta M$, the mass-luminosity relation approximately gives

$$\frac{L}{L_{\odot}} \approx \left(\frac{M}{M_{\odot}} \right)^4 \approx 1 + \frac{4\Delta M}{M_{\odot}}, \quad (48)$$

where L_{\odot} is the solar luminosity and M_{\odot} is the mass of the Sun (Duric, 2004). By relating the luminosity of a star to its mass, the Hertzsprung-Russell relation suggests a link between the luminosity and the gravitational power continuously dissipated inside the star.

The total solar luminosity is

$$L_{\odot} = 4\pi(1AU)^2 \times TSI = 3.827 \cdot 10^{26} W, \quad (49)$$

where 1 AU = 1.496 · 10¹¹ m is the average Sun-Earth distance, and TSI is the total solar irradiance 1360.94 W/m² at 1 AU. Every second, the core of the Sun transforms into luminosity a certain amount of mass according to the Einstein equation $E = mc^2$. If $dL(r)$ is the luminosity produced inside the shell between r and $r + dr$ (Bahcall et al., 2001, 2005), the mass transformed into light every second in the shell is

$$\frac{dm(r)}{dr} = \frac{1}{c^2} \frac{dL(r)}{dr}, \quad (50)$$

where $c = 2.998 \cdot 10^8$ m/s is the speed of the light and r is the distance from the center of the Sun.

The transformed material can be associated with a correspondent loss of gravitational energy of the star per time unit \dot{U}_\odot , which can be calculated using Eq. 50 as

$$\begin{aligned} \dot{U}_\odot &= \frac{1}{2} G \int_0^{R_S} m_\odot(r) \frac{dm(r)}{dr} \frac{1}{r} dr \\ &= \frac{1}{2} \frac{G}{c^2} \int_0^{R_S} m_\odot(r) \frac{dL(r)}{dr} \frac{1}{r} dr = 3.6 \cdot 10^{20} W \end{aligned} \quad (51)$$

where the initial factor 1/2 is due to the virial theorem, $m_\odot(r)$ is the solar mass within the radius $r \leq R_S$ and $L(r)$ is the luminosity profile function derived by the standard solar model (Bahcall et al., 2001, 2005).

The gravitational forces will do the work necessary to compensate for such a loss of energy to restore the conditions for the H-burning. In fact, the solar luminosity would decrease if the Sun's gravity did not fill the vacuum created by the H-burning, which reduces the number of particles by four ($4H \rightarrow 1He$). At the same time, the nucleus of He slowly sinks releasing additional potential energy. All this corresponds to a gravitational work in the core per time unit, $\dot{\Omega}_\odot$, that is associated with light production.

The basic analogy made by Scafetta (2012b) is that $\dot{\Omega}_\odot$ should be of the same order of magnitude as the rate of the gravitational energy loss due to H-fusion ($\dot{\Omega}_\odot \approx \dot{U}_\odot$). Moreover, the energy produced by the dissipation of the tidal forces in the core should be indistinguishable from the energy produced by the other gravitational forces in the Sun. Thus, it is as if tides added some gravitational power that becomes $\dot{\Omega}_\odot + \dot{\Omega}_{tidal}$.

For small perturbations, since light production is directly related both to the solar mass and to the gravitational power dissipated inside the core, Scafetta (2012b) assumed the equivalence

$$\frac{\Delta M}{M_\odot} \equiv \frac{\dot{\Omega}_{tidal}}{\dot{\Omega}_\odot}, \quad (52)$$

where $\dot{\Omega}_{tidal}$ is the tidal perturbing power dissipated inside the Sun and $\dot{\Omega}_\odot \equiv \dot{U}_\odot$ is the rate of the gravitational energy lost by the Sun through H-burning. Thus, from Eqs. 47 and 48 we get

$$L(t) \approx L_\odot + \frac{4L_\odot}{\dot{\Omega}_\odot} \dot{\Omega}_{tidal}(t) = L_\odot + A \cdot \dot{\Omega}_{tidal}(t), \quad (53)$$

where the amplification factor is

$$A = 4 \frac{L_\odot}{\dot{\Omega}_\odot} \approx 4 \frac{L_\odot}{U_\odot} \approx 4.25 \cdot 10^6. \quad (54)$$

Eq. 54 means that any little amount of gravitational power dissipated in the core (like that induced by planetary tidal forcing) could be amplified by a factor of the order of one million by nuclear fusion. This could be equivalent to having gravitational tidal amplitudes amplified from 1 mm to 1 kilometer at the tachocline. This amplification could solve the problem of the ‘‘homeopathic’’ gravitational tidal energy contribution highlighted by Charbonneau (2022).

By using such a large amplification factor the estimated gravitational power $\dot{\Omega}_{tidal}$ dissipated inside the solar core, Scafetta (2012b) calculated the tidally-induced TSI produced by each of the planets (Figure 9A and B), as well as that of all the planets together (Figure 9C). The sequence of the relative tidal relevance of the planets is Jupiter, Venus, Earth, Mercury, Saturn, Mars, Uranus and Neptune. The mean enhancement of their overall tidally-induced TSI is of the order of 0.3-0.8 W/m^2 , depending on the specific Love number of the tides (see Figure 9C). However, on shorter time scales the tides could produce TSI fluctuations up to 0.6-1.6 W/m^2 in absence of dampening mechanisms. In particular, on a decadal time scale, the TSI fluctuations due to Jupiter and Saturn could reach amplitudes of 0.08-0.20 W/m^2 (see the black curve in Figure 9C).

If the luminosity flux reaching the tachocline from the radiative zone is modulated by the contribution of tidally-induced luminosity oscillations with a TSI amplitude of the order of 0.01-0.10 W/m^2 , the perturbation could be sufficiently energetic to tune the solar dynamo with the planetary frequencies. The dynamo would then further amplify the luminosity signal received at the tachocline up to ~ 1 W/m^2 amplitudes as observed in TSI cycles (Willson and Mordvinov, 2003).

Figure 9D compares the periodograms of the sunspot number record and of the planetary luminosity signal shown in Figure 9C. The two side frequency peaks at about 10 years (J/S-spring tide) and 11.86 years (J-tide) perfectly coincide in the two spectral analyses. The central frequency peak at about 10.87 years shown only by sunspot numbers could be directly generated by the solar dynamo excited by the two tidal frequencies (Scafetta, 2012a) or other mechanisms connected with the dynamo as discussed above.

An obvious objection to the above approach is that the Kelvin-Helmholtz time-scale (Mitalas and Sills, 1992; Stix, 2003) predicts that the light journey from the core to the convective zone requires 10^4 to 10^8 years. Therefore, the luminosity fluctuations produced inside the core could be hardly detectable because they would be smeared out before reaching the convective zone. At most, there could exist only a slightly enhanced solar luminosity related to the overall tidally-induced TSI mean enhancement of the order of 0.3-0.8 W/m^2 as shown in Figure 9C.

However, several different mechanisms may be at work. In fact, the harmonic tidal forcing acts simultaneously throughout the core and in the radiative zone

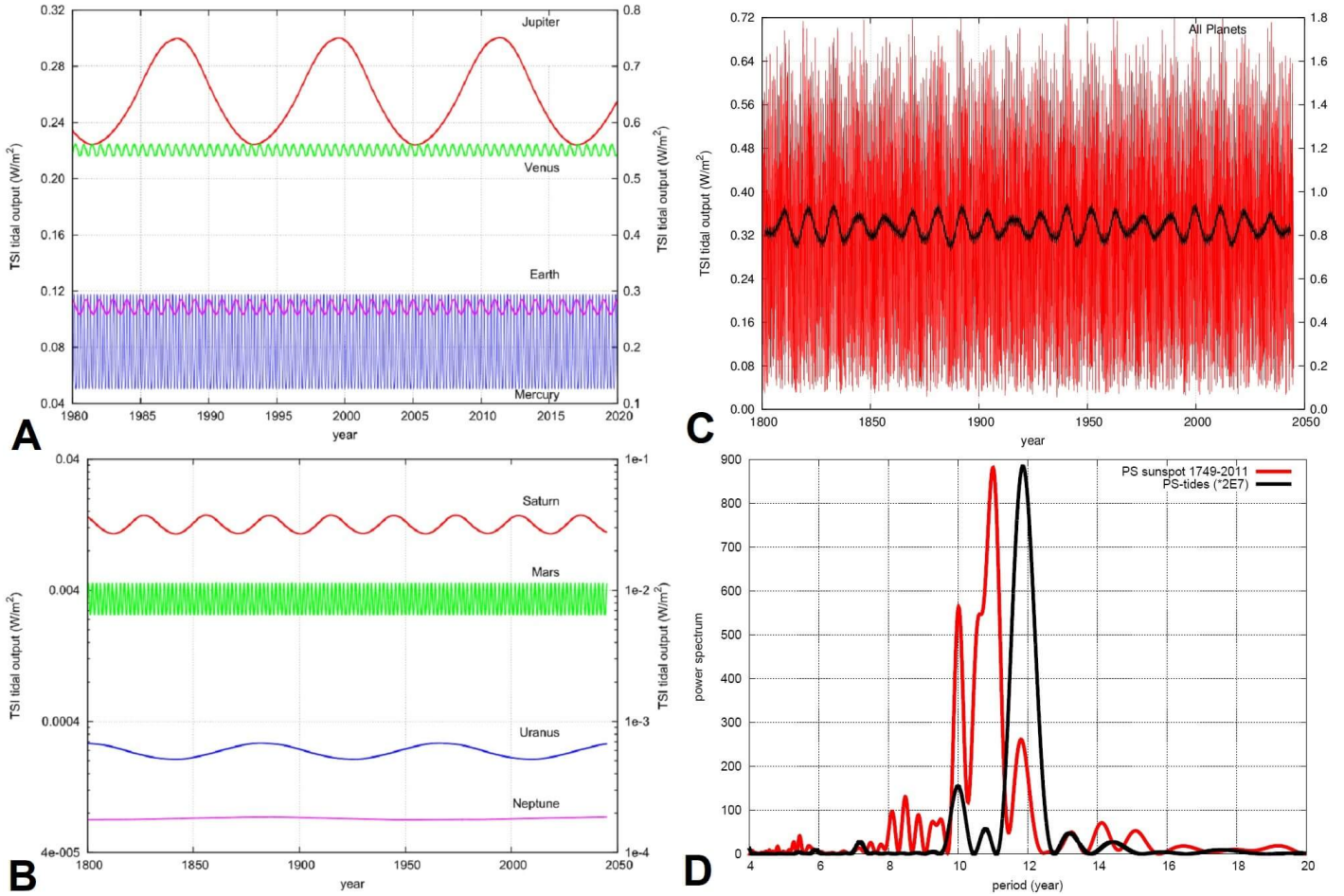


Figure 9: [A-B] Theoretical TSI enhancement induced by the tides of each planet on the Sun obtained using Scafetta (2012b) amplification hypothesis; the Love numbers are $3/2$ (left axis) and $15/4$ (right axis). [C] The same as produced by the tides of all the planets. [D] Lomb-periodogram spectral analysis of the sunspot number record (red) and of the tidal function (black) produced by all the planets.

, and simultaneously produces everywhere a synchronized energy oscillation that can be amplified in the core as discussed above. This would give rise to modulated seismic waves (g and p-mode oscillations) that can propagate from the inner core up to the tachocline region in a few hours because the sound speed inside the Sun is a few hundred kilometers per second (Hartlep and Mansour, 2005; Ahuir et al., 2021; Barker and Ogilvie, 2010). These waves might also couple with the g-waves produced in the tachocline (Goodman and Dickson, 1998) producing a in the tachocline region sufficiently strong to synchronize the solar dynamo with the planetary tidal frequencies.

11 Conclusion

Many empirical evidences suggest that planetary systems can self-organize in synchronized structures although some of the physical mechanisms involved are still debated.

We have shown that the high synchronization of our

own planetary system is nicely revealed by the fact that the ratios of the orbital radii of adjacent planets, when raised to the $2/3$ rd power, express the simple ratios found in harmonic musical consonances while those of the mirrored ones follow the simple, elegant, and highly precise scaling-mirror symmetry Eq. 1 (Bank and Scafetta, 2022).

The solar system is made of synchronized coupled oscillators because it is characterized by a set of frequencies that are linked to each other by the harmonic Eq. 3, which are easily detected in the solar wobbling. Thus, it is then reasonable to hypothesize that the solar activity could be also tuned to planetary frequencies.

We corroborated this hypothesis by reviewing the many planetary harmonics and orbital invariant inequalities that characterize the planetary motions and observing that often their frequencies correspond to those of solar variability.

It may be objected that, since the identified planetary frequencies are so numerous, it could be easy to occasionally find that some of them roughly correspond to those of the solar cycles. However, the fact is that

the planetary frequencies of the solar system, from the monthly to the millennial time scales, are not randomly distributed but tend to cluster around some specific values that quite well match those of the main solar activity.

Thus, it is rather unlikely that the results shown in Figures 3-7 are just occasional. In some cases, our proposed planetary models have even been able to predict the time-phase of the solar oscillations like that of the Schwabe 11-year sunspot cycle throughout the last three centuries, as well as those of the secular and millennial modulations throughout the Holocene. The two main planetary models that could explain the Schwabe 11-year cycle and its secular and millennial variation involve the planets Venus, Earth, Jupiter and Saturn, as it was initially suggested by Wolf (1859). We further suggest that the Venus-Earth-Jupiter model and the Jupiter-Saturn model could be working complementary to each other.

The alternative hypothesis that the solar activity is regulated by an unforced internal dynamics alone (i.e. by an externally unperturbed solar dynamo) has never been able to reproduce the variety of the observed oscillations. In fact, standard MHD dynamo models are not self-consistent and do not directly explain the well-known 11-year solar cycle nor they are able to predict its timing without assuming a number of calibrated parameters (Jiang et al., 2007; Tobias, 2002).

There have been several objections to a planetary theory of solar variability. For example, Smythe and Eddy (1977) claimed that planetary cycles and conjunctions could not predict the timing of grand solar minima, like the Maunder Minimum of the 17th century. However, Scafetta (2012a) developed a solar-planetary model able to predict all the grand solar maxima and minima of the last millennium (Figure 5).

Other authors reasonably claimed that planetary gravitational tides are too weak to modulate solar activity (Charbonneau, 2002; Jager and Versteegh, 2005; Charbonneau, 2022); yet, several empirical evidences support the importance of their role (Abreu et al., 2012; Scafetta, 2012b; Stefani et al., 2016, 2019; Wolff and Patrone, 2010). Stefani et al. (2016, 2021) proposed that the Sun could be at least synchronized by the tides of Venus, Earth and Jupiter producing an 11.07-year cycle that reasonably fits the Schwabe cycle. Longer cycles could be produced by a dynamo excited by angular momentum transfer from Jupiter and Saturn. Instead, Scafetta (2012b) proposed that, in the solar core, the effects of the weak tidal forces could be amplified one million times or more due to an induced increase in the H-burning, thus providing a sufficiently strong forcing to synchronize and modulate the solar dynamo with planetary harmonics at multiple time scales.

Objections to the latter hypothesis, based on the slow light propagation inside the radiative zone according to the Kelvin–Helmholtz timescale (Mitalas and Sills, 1992; Stix, 2003), could be probably solved. In fact, tidal

forces are believed to favor the onset of g-waves moving back and forth throughout the radiative region of the Sun (Ahuir et al., 2021; Barker and Ogilvie, 2010). Thus, g-waves themselves could be amplified and modulated in the core by the tidally induced H-burning enhancement (Scafetta, 2012b). Then, both tidal torques and g-waves could cyclically affect the tachocline region at the bottom of the convective zone and synchronize the solar dynamo.

Alternatively, planetary alignments can also modify the large-scale electromagnetic and gravitational structure of the planetary system altering the space weather in the solar system. For example, in coincidence of planetary alignments, an increase of solar flares has been observed (Hung, 2007; Bertolucci et al., 2017; Petrakou, 2021). The solar wobbling, which reflects the motion of the barycenter of the planets, changing from more regular to more chaotic trajectories, correlates well with some long climate cycles like the Bray-Hallstatt cycle (2100-2500 years) (Charvátová, 2000; Charvátová and Hejda, 2014; Scafetta et al., 2016). Finally, Scafetta et al. (2020) showed that the infalling meteorite flux on the Earth presents a 60-year oscillation coherent with the variation of the eccentricity of Jupiter’s orbit induced by Saturn. The falling flux of meteorites and interplanetary dust would then contribute to modulate cloud formation.

In conclusion, much empirical evidence suggests that planetary oscillations should be able to modulate the solar activity and even the Earth’s climate, although several open physical issues remain open. These results stress the importance of identifying the relevant planetary harmonics, the solar activity cycles and the climate oscillations as phenomena that, in many cases, are interconnected. This approach could be useful to predict both solar and climate variability using harmonic constituent models as it is currently done for oceanic tides. We think that the theory of a planetary modulation of solar activity should be further developed because no clear alternative theory exists to date capable to explain the observed planetary-solar interconnected periodicities.

Author Contributions

NS wrote the initial draft and prepared the figures. NS and AB contributed to the discussion and the revision of the submitted version.

Conflict of Interest

The authors declare that the research was conducted in the absence of any commercial or financial relationships that could be construed as a potential conflict of interest.

References

- Abreu, J. A., Beer, J., Ferriz-Mas, A., McCracken, K. G., and Steinhilber, F. (2012). Is there a planetary influence on solar activity? *Astron. Astrophys.* 548, A88. doi:10.1051/0004-6361/201219997
- Albert, C., Ferriz-Mas, A., Gaia, F., and Ulzega, S. (2021). Can Stochastic Resonance Explain Recurrence of Grand Minima? *ApJL* 916, L9.
- Agnihotri, R., and Dutta, K. (2003). Centennial scale variations in monsoonal rainfall (Indian, east equatorial and Chinese monsoons): manifestations of solar variability. *Current Science* 85, 459–463.
- Agol, E., Dorn, C., Grimm, S. L., Turbet, M., Ducrot, E., Delrez, L., et al. (2021). Refining the Transit-timing and Photometric Analysis of TRAPPIST-1: Masses, Radii, Densities, Dynamics, and Ephemerides. *Planetary Science Journal* 2, 1.
- Ahuir, J., Mathis, S., Amard L. 2021. Dynamical tide in stellar radiative zones. *Astronomy & Astrophysics* 651, A3.
- Aschwanden, M. J. (2018). Self-organizing systems in planetary physics: Harmonic resonances of planet and moon orbits. *New Astronomy* 58, 107–123.
- Bahcall J. N., Pinsonneault M. H., and Basu S. (2001). Solar models: current epoch and time dependences, neutrinos, and helioseismological properties. *Astrophysical Journal* 555, 990–1012.
- Bahcall J. N., Serenelli A., and Basu S. (2005). New solar opacities, abundances, helioseismology, and neutrino fluxes. *Astrophysical Journal* 621, L85–L88.
- Bank, M. J., and Scafetta, N. (2022). Scaling, Mirror Symmetries and Musical Consonances Among the Distances of the Planets of the Solar System. *Front. Astron. Space Sci.* 8:758184. doi: 10.3389/fspas.2021.758184
- Bard, E., Raisbeck, G., Yiou, F., and Jouzel J. (2000). Solar irradiance during the last 1200 years based on cosmogenic nuclides. *Tellus* 52B, 985–992.
- Barker, A. J., Ogilvie, G.I. (2010). On internal wave breaking and tidal dissipation near the centre of a solar-type star. *Monthly Notices of the Royal Astronomical Society* 404, 1849–1868.
- Bartels, J. (1934). Twenty-seven day recurrences in terrestrial-magnetic and solar activity, 1923–1933. *J. Geophysical Research* 39, 201-202a, doi: 10.1029/TE039i003p00201.
- Battistini, A. (2011). Il ciclo undecennale del sole secondo Bendandi (The 11-year solar cycle according to Bendandi). *New Ice Age*, <http://daltonsin minima.altervista.org/?p=8669>.
- Beck, J. (2000). A comparison of differential rotation measurements. *Solar Physics*. 191: 47–70.
- Beer, J., Tobias, S.M., Weiss, N.O. (2018). On long-term modulation of the Sun’s magnetic cycle. *Mon. Not. R. Astron. Soc.* 473, 1596–1602.
- Bendandi, R. (1931). *Un principio fondamentale dell’Universo* (A fundamental principle of the Universe), Faenza, Osservatorio Bendandi.
- Bertolucci, S., Zioutas, K., Hofmann, S., and Maroudas, M. (2017). The Sun and its planets as detectors for invisible matter. *Physics of the Dark Universe* 17, 13. doi:10.1016/j.dark.2017.06.001
- Bigg E.K. (1967). Influence of the planets Mercury on Sunspots. *The Astronomical Journal* 72, 463–466.
- Bollinger, C. J. (1952). A 44.77 year Jupiter-Earth-Venus configuration Sun-tide period in solar-climate cycles. *Academy of Science for 1952 – Proceedings of the Oklahoma*, 307–311. (http://digital.library.okstate.edu/oas/oas_pdf/v33/v307_311.pdf)
- Brown, E. W. (1900). A Possible Explanation of the Sun-spot Period. *Monthly Notices of the Royal Astronomical Society* 60, 599–606.
- Bucha, V., Jakubcová, I., and Pick, M. (1985). Resonance frequencies in the Sun’s motion. *Studia Geophysica et Geodaetica* 29, 107–111.
- Charbonneau, P. (2002). The rise and fall of the first solar cycle model. *Journal for the History of Astronomy* 33(4), 351–372.

- Charbonneau P. (2020). Dynamo Models of the Solar Cycle. *Living Rev. Sol. Phys.* 17, 4.
- Charbonneau P (2022) External Forcing of the Solar Dynamo. *Front. Astron. Space Sci.* 9:853676.
- Cauquoin, A., Raisbeck, G. M., Jozel, J., Bard, E., and ASTER Team (2014). No evidence for planetary influence on solar activity 330000 years ago. *Astron. Astrophys.* 561, A132.
- Chang, S., and Yu, Z. (1981). Historical records of meteorite falls in China and their time series analysis. *National Institute of Polar Research, Memoirs, Special Issue 20*, 276–284, 1981.
- Charvátová, I. (2000). Can origin of the 2400-year cycle of solar activity be caused by solar inertial motion? *Ann. Geophys.* 18, 399–405. doi:10.1007/s00585-000-0399-x, 2000.
- Charvátová, I., and Hejda, P. (2014). Responses of the basic cycle of 178.7 years and 2402 years in solar-terrestrial phenomena during Holocene. *Pattern Recogn. Phys.*, 2, 21–26. doi:10.5194/PRP-2-21-2014
- Cionco, R. G., Pavlov, D. A. (2018). Solar barycentric dynamics from a new solar-planetary ephemeris. *Astron. Astrophys.* 615, A153.
- Cionco, R. G., Kudryavtsev, S. M., Soon, W. W.-H. (2021). Possible origin of some periodicities detected in solar-terrestrial studies: Earth’s orbital movements. *Earth and Space Science* 8, e2021EA001805.
- Cole, L. C., Bushby, P. J. (2014). Modulated cycles in an illustrative solar dynamo model with competing α -effects. *Astronomy & Astrophysics* 563, A116.
- de Vries, H. (1958). Variations in concentration of radiocarbon with time and location on Earth. *Proc. K. Ned. Akad. Wet. B*, 61, 94–102.
- Dicke, R.H. (1978). Is there a chronometer hidden deep in the Sun? *Nature* 276, 676.
- Dikpati, M., Gilman, P. A. (2007). Global solar dynamo models: simulations and predictions of cyclic photospheric fields and long-term non-reversing interior fields. *New J. Phys.* 9, 297.
- Dikpati, M., Cally, P.S., McIntosh, S.W., Heifetz, E.: 2017, The origin of the “seasons” in space weather. *Sci. Rep.* 7, 14750.
- Duric N. (2004). *Advanced astrophysics*, Cambridge University Press. pp. 19.
- Eyring, V., Bony, S., Meehl, G.A., *et al.* (2016). Overview of the Coupled Model Intercomparison Project Phase 6 (CMIP6) experimental design and organization. *Geoscientific Model Development*, 9 (5), 1937–1958. <https://doi.org/10.5194/gmd-9-1937-2016>
- Etz, D. V. (2000). Conjunctions of Jupiter and Saturn. *Journal of the Royal Astronomical Society of Canada* 94, 174–178.
- Fairbridge, R. W., Shirley, J. H. (1987). Prolonged minima and the 179-yr cycle of the solar inertial motions. *Solar Phys.* 110, 191–210.
- Fröhlich, C. (2006). Solar irradiance variability since 1978: revision of the PMOD composite during solar cycle 21. *Space Science Reviews* 125, 53–65.
- Geddes, A.B., King-Hele, D.G. (1983). Equations for mirror symmetries among the distances of the planets. *Quarterly Journal of the Royal Astronomical Society* 24, 10–13.
- Godwin, J. (1992). *The Harmony of the Spheres: The Pythagorean Tradition in Music*. Inner Traditions, Rochester, Vermont USA.
- Goldreich, P., Nicholson, P. (1989). Tidal Friction in Early-Type Stars. *Astrophysical Journal* 342, 1079–1084.
- Goodman, J., Dickson, E.S. (1998). Dynamical Tide in Solar-Type Binaries . *Astrophysical Journal* 507, 938–944.
- Gurgenashvili, E., Zaqarashvili, T. V., Kukhianidze, V., Reiners, A., Reinhold, T., Lanza, A. F. (2022). Rieger-type cycles on the solar-like star KIC 2852336. *Astronomy & Astrophysics* 660, A33.
- ter Haar, D. (1948). Recent theories about the origin of the solar system. *Science New Series*, 107, 405–411.
- Hale, G. E. (1908). On the probable existence of a magnetic field in sun-spots. *The Astrophysical Journal* 28: 315.

- Hartlep T., Mansour N. N. (2005). Acoustic wave propagation in the Sun. Center for Turbulence Research Annual Research Briefs, Stanford University, pp. 357–365.
- Hung, C.-C. (2007). Apparent Relations Between Solar Activity and Solar Tides Caused by the Planets. *NASA report /TM- 2007-214817*. Available at: <http://ntrs.nasa.gov/search.jsp?R=20070025111>.
- de Jager C., and Versteegh G. J. M. (2005). Do Planetary Motions Drive Solar Variability? *Solar Physics* 229, 175–179.
- Jakubcová, I., and Pick, M. (1986). The planetary system and solar-terrestrial phenomena. *Studia Geophysica et Geodaetica* 30, 224–235.
- Jiang, J., Chatterjee, P., Choudhuri, A. R. (2007). Solar activity forecast with a dynamo model. *Monthly Notices of the Royal Astronomical Society* 381, 1527–1542.
- Jose, P. D. (1965). Sun’s motion and sunspots, *Astrophysical Journal* 70, 193. doi:10.1086/109714
- Keeling, C. D., Whorf, T. P. (2000). The 1,800-year oceanic tidal cycle: A possible cause of rapid climate change. *PNAS* 97 (8), 3814–3819.
- Kepler, J. (1606). *De Stella Nova in Pede Serpentarii*, Typis Pauli Sessii, Pragmae.
- Kerr, R. A. (2001). A variable sun paces millennial climate. *Science* 294, 1431–1433.
- Kopp, G., and Lawrence, G. (2005a). The Total Irradiance Monitor (TIM): Instrument; Design. *Solar Physics* 230, 91–109.
- Kopp, G., Heuerman, K., and Lawrence, G. (2005b). The Total Irradiance Monitor; (TIM): Instrument Calibration. *Solar Physics* 230, 111–127.
- Kotov, V.A. (2020). Rotation anomaly of the Sun. *Astron. Nachr.* 341, 588– 594.
- Kotov, V.A., Haneychuk, V.I. (2020). Oscillations of solar photosphere: 45 years of observations. *Astron. Nachr.* 341, 595-599.
- Landscheidt, T. (1999). Extrema in sunspot cycle linked to Sun’s motion. *Solar Physics* 189, 415–426.
- Ljungqvist F. C. (2010). A new reconstruction of temperature variability in the extra-tropical Northern Hemisphere during the last two millennia. *Geografiska Annaler Series A* 92, 339–351.
- Lovett, E. O. (1895). The Great Inequality of Jupiter and Saturn. *Astronomical Journal*, 351, 113–127.
- Lüdecke, H.-J., Weiss, C.O., Hempelmann, A. (2015). Paleoclimate forcing by the solar De Vries/Suess cycle. *Clim. Past Discuss.* 11, 279-305.
- Macario-Rojas, A., Smith, K. L., Roberts, P. C. E. (2018). Solar activity simulation and forecast with a flux-transport dynamo. *MNRAS* 479, 3791–3803.
- McCracken, K. G., Dreschhoff, G. A., Smart, D. F., and Shea, M. A. (2001). Solar cosmic ray events for the period 1561-1994: 2. The Gleissberg periodicity. *Geophys. Res. Lett.* 106, 21599. doi:10.1029/2000JA000238
- McCracken, K. G., Beer, J., Steinhilber, F., and Abreu, J. (2013). A phenomenological study of the cosmic ray variations over the past 9400 years, and their implications regarding solar activity and the solar dynamo. *Solar Physics* 286, 609. doi:10.1007/s11207-013-0265-0
- Morice, C. P., Kennedy, J. J., Rayner, N. A., and Jones, P. D. (2012). Quantifying uncertainties in global and regional temperature change using an ensemble of observational estimates: the HadCRUT4 dataset. *J. Geophys. Res.* 117, D08101.
- Mörner, N.-A., Scafetta, N., Solheim, J.-E. (2015). The January 7 Giant Solar Flare, the Simultaneous Triple Planetary Conjunction and Additional Records at Tromsø, Northern Norway. In “*Planetary Influence on the Sun and the Earth, and a Modern Book-Burning.*” pp. 33–38, Nova Science Publisher, New York. ISBN: 9781634828376
- Mitalas, R., and Sills, K. (1992). On the photon diffusion time scale for the sun. *The Astrophysical Journal* 401, 759–760.

- Moons, M., and Morbidelli, A. (1995). Secular resonances inside mean-motion commensurabilities: the 4/1, 3/1, 5/2 and 7/3 cases. *Icarus* 114, 33–50.
- NASA News (2014). Sun unleashes first X-class flare of 2014. Jan. 7. Available at: <http://svs.gsfc.nasa.gov/vis/a010000/a011100/a011136/>
- Neff, U., Burns, S. J., Mangini, A., Mudelsee, M., Fleitmann, D. and Matter, A. (2001). Strong coherence between solar variability and the monsoon in Oman between 9 and 6 kyear ago. *Nature* 411, 290. doi:10.1038/35077048
- Ogurtsov, M. G., Nagovitsyn, Y. A., Kocharov, G. E., and Jungner, H. (2002). Long-period cycles of the sun's activity recorded in direct solar data and proxies. *Solar Physics* 211, 371–394.
- Parker, E. N. (1955). Hydromagnetic Dynamo Models. *Astrophysical Journal*, 122, 293–314.
- Parker, E. N. (1958). Dynamics of the Interplanetary Gas and Magnetic Fields. *Astrophysical Journal*, 128, 664–676.
- Petrakou, E. (2021). Planetary statistics and forecasting for solar flares. *Advances in Space Research* 68, 2963–2973. doi: 10.1016/j.asr.2021.05.034
- Pikovsky, A., Roseblum, M., Kurths, J. (2001). *Synchronization: A Universal Concept in Nonlinear Sciences*. Cambridge University Press.
- Press, W. H., Teukolsky, S. A., Vetterling, W. T., and Flannery, B. P. (1997). *Numerical Recipes in C, 2nd Edn.*, Cambridge University Press.
- Reimer, P. J., Baillie, M. G. L., Bard, E., et al. (2004). Intcal04 terrestrial radiocarbon age calibration, 0–26 cal kyear BP. *Radiocarbon* 46, 1029. doi:10.1017/S0033822200032999. Available at <https://www.radiocarbon.org/IntCal04.htm>
- Salvador, R. J. (2013). A mathematical model of the sunspot cycle for the past 1000 year. *Pattern Recogn. Phys.* 1, 117–122. doi:10.5194/prp-1-117-2013.
- Scafetta, N., Grigolini, P., Imholt, T., Roberts, J. A., and West, B. J. (2004). Solar turbulence in earth's global and regional temperature anomalies. *Physical Review E*, 69, 026303.
- Scafetta, N., and West, B. J. (2006). Phenomenological solar signature in 400 years of reconstructed Northern Hemisphere temperature record. *Geophysical Research Letters*, 33, L17718.
- Scafetta, N. (2009). Empirical analysis of the solar contribution to global mean air surface temperature change. *Journal of Atmospheric and Solar-Terrestrial Physics* 71, 1916–1923.
- Scafetta, N. (2010). Empirical evidence for a celestial origin of the climate oscillations and its implications. *Journal of Atmospheric and Solar-Terrestrial Physics* 72, 951–970. doi:10.1016/j.jastp.2010.04.015, 2010.
- Scafetta, N. (2011). Total solar irradiance satellite composites and their phenomenological effect on climate. In *Evidence-Based Climate Science*. (Easterbrook D., Elsevier), 12, 289–316.
- Scafetta, N. (2012a). Multi-scale harmonic model for solar and climate cyclical variation throughout the Holocene based on Jupiter-Saturn tidal frequencies plus the 11 year solar dynamo cycle. *Journal of Atmospheric and Solar-Terrestrial Physics* 80, 296–311. doi:10.1016/j.jastp.2012.02.016, 2012a.
- Scafetta, N. (2012b). Does the Sun work as a nuclear fusion amplifier of planetary tidal forcing? A proposal for a physical mechanism based on the mass-luminosity relation. *Journal of Atmospheric and Solar-Terrestrial Physics* 81–82, 27–40. doi:10.1016/j.jastp.2012.04.002.
- Scafetta, N. (2012c). A shared frequency set between the historical mid-latitude aurora records and the global surface temperature. *Journal of Atmospheric and Solar-Terrestrial Physics* 74, 145–163.
- Scafetta, N. (2012d). Testing an astronomically based decadal-scale empirical harmonic climate model versus the IPCC (2007) general circulation climate models. *Journal of Atmospheric and Solar-Terrestrial Physics* 80, 124–137.
- Scafetta, N. (2013). Discussion on climate oscillations: CMIP5 general circulation models versus a semi-empirical harmonic model based on astronomical cycles. *Earth-Sci. Rev.* 126, 321–357.
- Scafetta, N., and Willson, R. C. (2013a). Planetary harmonics in the historical Hungarian aurora record (1523–1960). *Planet. Space Sci.* 78, 38–44. doi:10.1016/j.pss.2013.01.005, 2013a.

- Scafetta, N., and Willson, R. C. (2013b). Empirical evidences for a planetary modulation of total solar irradiance and the TSI signature of the 1.09 year Earth-Jupiter conjunction cycle. *Astrophys. Space Sci.* 348, 25–39. doi:10.1007/s10509-013-1558-3.
- Scafetta, N., and Willson, R. C. (2013c). Multiscale comparative spectral analysis of satellite total solar irradiance measurements from 2003 to 2013 reveals a planetary modulation of solar activity and its nonlinear dependence on the 11 year solar cycle. *Pattern Recognition in Physics* 1, 123–133. doi:10.5194/prp-1-123-2013.
- Scafetta, N. (2014a). The Complex Planetary Synchronization Structure of the Solar System. *Pattern Recognition in Physics* 2, 1–19. doi:10.5194/prp-2-1-2014
- Scafetta, N. (2014b). Discussion on the spectral coherence between planetary, solar and climate oscillations: a reply to some critiques. *Astrophysics and Space Science*, 354, 275–299. doi:10.1007/s10509-014-2111-8
- Scafetta, N. (2014c). Multi-scale dynamical analysis (MSDA) of sea level records versus PDO, AMO, and NAO indexes. *Climate Dynamics* 43, 175–192.
- Scafetta, N. (2016). High resolution coherence analysis between planetary and climate oscillations. *Advances in Space Research* 57(10), 2121–2135.
- Scafetta, N., Milani, F., Bianchini, A., and Ortolani, S. (2016). On the astronomical origin of the Hallstatt oscillation found in radiocarbon and climate records throughout the Holocene. *Earth-Sci. Rev.* 162, 24. doi:10.1016/j.earscirev.2016.09.004
- Scafetta, N. (2018). Reply on Comment on “High resolution coherence analysis between planetary and climate oscillations” by S. Holm. *Advances in Space Research* 62, 334–342.
- Scafetta, N., Milani, F., Bianchini, A. (2019a). Multiscale Analysis of the Instantaneous Eccentricity Oscillations of the Planets of the Solar System from 13,000 BC to 17,000 AD. *Astronomy Letters* 45(11), 778–790.
- Scafetta, N., Willson, R. C., Lee, J. N., and Wu, D. L. (2019b). Modeling quiet solar luminosity variability from TSI satellite measurements and proxy models during 1980-2018. *Remote Sensing*, 11(21), 2569.
- Scafetta, N., Milani, F., Bianchini, A. (2020). A 60-Year Cycle in the Meteorite Fall Frequency Suggests a Possible Interplanetary Dust Forcing of the Earth’s Climate Driven by Planetary Oscillations. *Geophysical Research Letters*, 47(18), e2020GL089954.
- Scafetta, N. (2020). Solar Oscillations and the Orbital Invariant Inequalities of the Solar System. *Solar Physics* 295, 33. doi:10.1007/s11207-020-01599-y
- Scafetta, N. (2021). Reconstruction of the Interannual to Millennial Scale Patterns of the Global Surface Temperature. *Atmosphere*, 12, 147.
- Schwabe H. (1843). Sonnenbeobachtungen im Jahre 1843" [Observations of the sun in the year 1843]. *Astronomische Nachrichten* 21, 233–236.
- Shkolnik, E., Walker, G. A. H., and Bohlender D. A. (2003). Evidence for Planet-induced Chromospheric Activity on HD 179949. *The Astrophysical Journal* 556, 296–301.
- Shkolnik, E., Walker, G. A. H., Bohlender, D. A., Gu P.-G., and Kurster, M. (2005). Hot Jupiters and Hot Spots: The Short- and Long-Term Chromospheric Activity on Stars with Giant Planets. *The Astrophysical Journal* 622, 1075–1090.
- Smythe, C. M., Eddy, J. A. (1977). Planetary tides during Maunder sunspot. *Nature* 266, 434–435.
- Solheim, J.-E. (2013). The sunspot cycle length – modulated by planets? *Pattern Recognition in Physics* 1, 159–164. doi:10.5194/prp-1-159-2013.
- Stefani, F., Weber, N., Weier, T., and Giesecke, A. (2016). Synchronized helicity oscillations: A link between planetary tides and the solar cycle? *Solar Physics* 291, 2197.
- Stefani, F., Giesecke, A., Weber, N., Weier, T. (2018). On the synchronizability of Tayler-Spruit and Babcock-Leighton type dynamos. *Solar Physics* 293, 12.
- Stefani, F., Giesecke, A., Weier, T. (2019). A model of a tidally synchronized solar dynamo. *Solar Physics* 294, 60.

- Stefani, F., Beer, J., Giesecke, A., et al. (2020a). Phase coherence and phase jumps in the Schwabe cycle. *Astron. Nachr.* 20, 341, 600–615.
- Stefani, F., Giesecke, A., Seilmayer, M., Stepanov, R., Weier T. (2020b). Schwabe, Gleissberg, Suess-de Vries: Towards a consistent model of planetary synchronization of solar cycles. *Magnetohydrodynamics* 56, No. 2/3, 269-280.
- Stefani, F., Stepanov, R., and Weier, T. (2021). Shaken and Stirred: When Bond Meets Suess-De Vries and Gnevyshev-Ohl. *Sol. Phys.* 296, 88.
- Stephenson, B. (1974). *The Music of the Heavens*. Princeton University Press, Princeton, NJ.
- Steinhilber F., Beer J., and Fröhlich C. (2009). Total solar irradiance during the Holocene. *Geophysics Research Letters* 36, L19704.
- Steinhilber, F., Abreu, J. A., Beer, J., Brunner, I., Christl, M., Fischer, H., Heikkila, U., Kubik, P. W., Mann, M., McCracken, K. G., Miller, H., Miyahara, H., Oerter, H., Wilhelms, F. (2012). 9,400 years of cosmic radiation and solar activity from ice cores and tree rings. *PNAS* 109(16), 5967–5971.
- Stix, M. (2003). On the time scale of energy transport in the sun. *Solar Physics* 212, 3–6.
- Stuiver, M., Reimer, P. J., Bard, E., Beck, J. W., Burr, G. S., Hughen, K. A., Kromer, B., McCormac, G., Van Der Plicht, J. and Spurk, M. (1998). INTCAL98 Radiocarbon age calibration, 24,000-0 cal BP. *Radiocarbon* 40, 1041. doi:10.1017/S0033822200019123
- Suess H. E. (1965). Secular variations of the cosmic-ray-produced carbon 14 in the atmosphere and their interpretations. *J. Geophys. Res.* 70, 5937–5952.
- Tattersall, R. (2013). The Hum: Lognormal distribution of Planetary-Solar resonance. *Pattern Recognition in Physics* 1, 185–198.
- Tobias, S. M. (2002). The solar dynamo. *Philosophical Transactions on the Royal Society A* 360(1801), 2741–2756.
- Vos, H., Brüchmann, C., Lücke, A., Negendank, J.F.W., Schleser, G.H., Zolitschka, B. (2004). Phase stability of the solar Schwabe cycle in lake Holzmaar, Germany, and GISP2, Greenland, between 10,000 and 9,000 cal. BP. In: Fischer, H., Kumke, T., Lohmann, G., Flöser, G., Miller, H., von Storch, H., Negendank, J.F. (eds.), *The Climate in Historical Times: Towards a Synthesis of Holocene Proxy Data and Climate Models*. GKSS School of Environmental Research, Springer, Berlin, 293.
- Wagner, G., Beer, J., Masarik, J., Muscheler, R., Kubik, P. W., Mende, W., Laj, C., Raisbeck, G. M., Yiou, F. (2001). Presence of the solar de Vries cycle (~205 years) during the last ice age. *Geophys. Res. Lett.* 28, 303-306.
- Weiss, N.O., Tobias, S.M. (2016). Supermodulation of the Sun’s magnetic activity: the effects of symmetry changes. *Mon. Not. Roy. Astron. Soc.* 456, 2654–2661.
- Wilson, I. R. G. (2013). The Venus–Earth–Jupiter spin–orbit coupling model, *Pattern Recognition in Physics* 1, 147–158, doi:10.5194/prp-1-147-2013.
- Willson, R. C., and Mordvinov, V. (1999). Time-Frequency Analysis of Total Solar Irradiance Variations. *Geophys. Res. Lett.* 26(24), 3613–3616. doi:10.1029/1999GL010700.
- Willson, R. C., and Mordvinov, V. (2003). Secular total solar irradiance trend during solar cycles 21-23. *Geophys. Res. Lett.* 30, 1199. doi:10.1029/2002GL016038.
- Wolf, R. (1859). Extract of a letter to Mr. Carrington. *Monthly Notices of the Royal Astronomical Society* 19, 85–86.
- Wyatt, M. G., and Curry, J. A. (2014). Role for Eurasian Arctic shelf sea ice in a secularly varying hemispheric climate signal during the 20th century. *Climate Dynamics* 42, 2763–2782.
- Wood, F. J. (1986). *Tidal Dynamics*, Reidel, Dordrecht, the Netherlands.
- Wolff, C. L., and Patrone, P. N. (2010). A new way that planets can affect the Sun. *Solar Physics* 266, 227. doi:10.1007/s11207-010-9628-y
- Yamaguchia Y., Yokoyamaa Y., Miyaharad H., Shoe K., and Nakatsukaf T., (2010). Synchronized Northern Hemisphere climate change and solar magnetic cycles during the Maunder Minimum. *PNAS* 107, 20697–20702.

- Yu, Z., Chang, S., Kumazawa, M., Furumoto, M., and Yamamoto, A. (1983). Presence of periodicity in meteorite falls. *National Institute of Polar Research, Memoirs*, Special Issue 30, 362–366.
- Zaqarashvili, T. V., Carbonell, M., Oliver, Ballster, J. L. (2010). Magnetic Rossby waves in the solar tachocline and Rieger-type periodicities. *The Astrophysical Journal* 709, 749–758.
- Zaqarashvili, T. V. (2018). Equatorial magnetohydrodynamic shallow water waves in the solar tachocline. *Astrophys. J.* 856, 32.
- Zaqarashvili, T. V., Albekioni, M., Ballester, J. L. et al. (2021). Rossby Waves in Astrophysics. *Space Sci Rev* 217, 15.
- Zioutas, K., Maroudas, M., Kosovichev, A. (2022). On the Origin of the Rhythmic Sun's Radius Variation. *Symmetry* 14, 325.